The Pennsylvania State University

The Graduate School

College of Engineering

FABRICATION AND CHARACTERIZATION OF HYDROGEL-FILLED NANOLIPOSOMES FOR APPLICATIONS IN NANOMEDICINE

A Thesis in

Bioengineering

by

Eric VanArsdale

Submitted in Partial Fulfillment
of the Requirements
for the Degree of

Master of Science

December 2015

The thesis of Eric VanArsdale was reviewed and approved* by the following:

Sheereen Majd
Assistant Professor of Biomedical Engineering
Thesis Advisor

Peter Butler
Associate Dean for Education in the College of Engineering
Professor of Biomedical Engineering

William Hancock
Professor of Biomedical Engineering
Graduate Program Officer

Chen Dong
Distinguished Professor of Biomedical Engineering
Head of the Department

*Signatures are on file in the Graduate School

ABSTRACT

Nano-scale carriers that enable selective delivery of bioactive payloads to specific cells are sought after in gene therapy, regenerative medicine, and cancer treatment. Nano-liposomes have emerged as the first successful generation of nano-carriers, headlined by the doxorubicin liposome formulations known as Doxil/Caelyx. Concerns with liposomal formulations are *in vivo* stability and rapid drug efflux from the liposome lumen. This thesis presents a simple modification to liposome drug formulations and evaluates changes to stability and release properties by inclusion of a hydrogel core within the intraliposomal space.

The resultant nanocarriers are evaluated for their size, surface charge, colloidal stability, and release properties. The presence of the hydrogel core is confirmed by membrane permeabilization by TX-100 detergent and cryogenic transmission electron microscopy. Two distinct drug molecules, rhodamine123 and doxorubicin, were encapsulated in the liposome and the liposome nanogels were monitored for drug release by dialysis against a large volume of PBS. The results showed that the addition of a hydrogel core allows for the use of lipid blends that were previously ineffective for drug retention in liposomal doxorubicin formulations. Taken together, this work suggests that the simple inclusion of a hydrogel polymer interior to nanoliposomes opens the door for a robust control over colloidal stability and release properties without significantly altering existing liposome fabrication protocols. The proposed approach is shown to be flexible enough to work alongside several existing technologies.

TABLE OF CONTENTS

List of Figures v

List of Tables viii

Acknowledgements ix

Chapter 1 Introduction 1

1.1 Nanoparticle Design 1
1.1.1 Size and Shape 2
1.1.2 Surface Charge and Stability 6
1.1.3 Elastic Toughness 10
1.1.4 Targeting Schemes and Controlled Release 12
1.2 Project Goals and Hypotheses 16

Chapter 2 Experimental Methods and Materials 20

2.1 Materials 20
2.2 Fabrication of Lipid Coated Nanogels 20
2.2.1 Formation and Sizing of Liposomes 21
2.2.2 Removal of Bulk Phase Photo initiator 21
2.2.3 Phosphatidyl Choline (PC) Assay 22
2.2.4 Ammonium Sulfate Gradient for Loading Doxorubicin 22
2.3 Nanoparticle Characterization 23
2.3.1 Size and Zeta Potential 23
2.3.2 Morphology 23
2.3.3 Stability in Biomimetic Environments 24
2.4 Doxorubicin Encapsulation and Release 24
2.4.1 Encapsulation Efficiency and Doxorubicin Gelation 24
2.4.2 Release Profile 25
2.4.3 Statistics and Significance 25

Chapter 3 Results and Discussion 26

3.1 Fabrication and Characterization of LNGs 26
3.1.1 Varying the PEGDA Content 27
3.1.2 Varying the Lipid Content 30
3.1.3 Varying the Extent of Sonication and Extrusion 35
3.1.4 Bulk Phase Photoinitiator Removal Protocols 38
3.1.5 Particle Morphology and the Hydrogel Core 39
3.1.6 Stability and Surface Charge 44
3.2 Encapsulation of Doxorubicin and Rhodamine123 46
3.2.1 Passive Encapsulation during Hydration of the Lipid Film 46
3.2.2 Ammonium Sulfate Gradient Encapsulation of Doxorubicin 50
3.2.3 Release of Doxorubicin from Polymerized Vesicles 54

Chapter 4 Future Research and Considerations 58

Bibliography 61

LIST OF FIGURES

Figure 1-1. *In vivo* data demonstrating the importance of fluidic stability of nanoparticles g.)Increasing elongation of the worm-like micelles (increases left to right) increase fluorescent accumulation at the tumor site. h.) Corresponding photon counts at the tumor site as a quantifiable measurement of concentration. Figure adapted from Jiang et al 3

Figure 1-2. Functional schematic of shape-dependent activation of membrane bound receptors a.) A depiction of the functional dimension, length (right) or radius (left), that corresponds to activation of receptors on the membrane as the receptor is engulfed by the cell. b.) A concentration gradient depiction of receptor activation and diffusion at the site of nanoparticle contact. Figure adapted from Wang et al. 5

Figure 1-3. An overview of the known endocytosis routes of entry into the intracellular space. Figure adapted from Mercer et al. 8

Figure 1-4. Inhibitor study of the influence of elasticity of nanogels on endocytosis mechanism. Bars left to right show increasing elasticity (20-200 kPA). Uptake in the presence of the identified inhibitor is presented as a percentage of the uptake of each particular particle formulation in standard medium. Sodium azide was used as an inhibitor for ATP-dependent endocytosis, amiloride was used as an inhibitor of micropinocytosis, chloropromazine was used as an inhibitor of clathrin-mediated endocytosis, nystatin was used as an inhibitor of cavaeloe mediated endocytosis, and nocodazole was used as an inhibitor of microtubule-associated endocytosis. Figure adapted from Banquay et al.....11

Figure 1-5. Schematic demonstration of selective gelation of hydrogels within a liposome template. The process is broken down three steps: (1) hydration of a lipid film with polymer solution, (2) sizing of the liposomes using extrusion, (3) and selective gelation using UV in the interior of the liposome. Figure adapted from An et al. 18

Figure 3-1. DOPC:Chol (85:15) vesicle size by PEGDA volume percentage. Error bars represent standard deviation and asterisks denote significant difference ($P < 0.05$). 32

Figure 3-2. POPC:Chol (85:15) vesicle size by PEGDA volume percentage. Error bars represent standard deviation and asterisks denote significant difference ($P < 0.05$). 33

Figure 3-3. DOPC:Chol:DSPE-PEG(2000) (80:15:5) vesicle size for liposomes and LNG particles (PEGDA 10% v/v). Error bars represent standard deviation and asterisks denote significant difference ($P < 0.05$) 34

Figure 3-4. POPC:Chol:DSPE-PEG(2000) (80:15:5) vesicle size for liposomes and LNG particles (PEGDA 10% v/v). Error bars represent standard deviation.....34

Figure 3-5. Cryo-TEM image of large DOPC:Chol:DSPE-PEG(2000) (80:15:5) multilamellar LNG vesicles (PEGDA 50%) prepared by 4 intervals of 1 minute exposure to tip sonication and 11 passes through a 100 nm membrane and an 80 nm membrane. 36

Figure 3-6. SEM image of an area in the center of a dried POPC:Chol (85:15) LNG particle (50% v/v PEGDA) sample on a microscope coverslip and sputter coated with Iridium.....40

Figure 3-7. SEM image of an area near the outer edge of a dried POPC:Chol (85:15) LNG particle (50% v/v PEGDA) sample on a microscope coverslip and sputter coated with Iridium. 40

Figure 3-8. Cryo-TEM image of DOPC:Chol:DSPE-PEG(2000) LNG particles (15% wt/wt) prepared with 4 intervals of 2 minutes exposure to a tip sonicator and extrusion through a 100 nm and 80 nm nanoporous filter.. 41

Figure 3-9. DLS size distribution of the three DOPC:Chol:DSPE-PEG(2000) LNG samples imaged. The red peak corresponds to Figure 3-8. 42

Figure 3-10. Cryo-TEM image of DOPC:Chol:DSPE-PEG(2000) LNG particles near the edge of the cooper grid.....42

Figure 3-11. DLS measurements of liposomes (a-b) and POPC:Chol:DSPE-PEG(2000) LNG particles (15% wt/wt) (c-d) in 15% TX-100. a.) DLS measurement of non-polymerized liposome prior to addition of detergent. b.) Liposome size measurement after addition of 15% TX-100 c.) DLS measurement of LNG particles prior to addition of detergent. d.) LNG particle size measurement after addition of 15% TX-100.....44

Figure 3-12 Average size measurements of POPC:Chol:DSPE-PEG(2000) LNG particles (15% wt/wt) in 50% FBS solution monitored over 5 days. Error bars represent standard deviation and asterisks denote the formation of large protein aggregates in solution. 45

Figure 3-13. Serum stability of LNG particles in 50% FBS. a.) Average size measurements of POPC:Chol:DSPE-PEG(2000) LNG particles (15% wt/wt) in 50% FBS solution monitored over 5 days. Error bars represent standard deviation and "Ag" denotes the formation of large protein aggregates in solution. b.) DLS measurement from day 1 c.) DLS measurement from day 5.....46

Figure 3-14. Encapsulation efficiency of rhodamine123 in POPC:Chol:DSPE-PEG(2000) (80:15:5) LNG particles (15% wt/wt) and liposomes. Error bars represent standard deviation.....48

Figure 3-15. Procedural loading efficiency of rhodamine123 in POPC:Chol:DSPE-PEG(2000) (80:15:5) LNG particles (15% wt/wt) and liposomes. Error bars represent standard deviation and asterisks denote significant difference ($P < 0.05$). 49

Figure 3-16. Encapsulation efficiency of doxorubicin versus incubation time for POPC:Chol:DSPE-PEG(2000) (80:15:5) LNG particles (15% wt/wt) pre-polymerization. 53

Figure 3-17. Encap Encapsulation of doxorubicin versus time using sodium chloride 0.15 M for POPC:Chol:DSPE-PEG(2000) (80:15:5) LNG particles (15% wt/wt) pre-polymerization. Values were normalized by the initial RFU reading. Error bars represent standard deviation.....54

Figure 3-18. Doxorubicin release POPC:Chol:DSPE-PEG(2000) (80:15:5) LNG particles (15% wt/wt) post-polymerization in 3L 1x PBS. Error bars represent standard deviation.....55

Figure 3-19. Doxorubicin crystal stability measured as a function of the 470/550 absorbance ratio during doxorubicin efflux from POPC:Chol:DSPE-PEG(2000) (80:15:5) LNG particles (15% wt/wt) post-polymerization. Data corresponds to Figure 3-17. Error bars represent standard deviation.....56

LIST OF TABLES

Table 3-1. Summary of POPC:Chol (85:15) vesicle fabrication data for samples prepared by extrusion and sonication. 15% wt/wt PEGDA LNGs contain POPC:Chol:DSPE-PEG(2000) (80:15:5).....28

Table 3-2. Summary of DOPC:Chol (85:15) vesicle fabrication data for samples prepared by extrusion and sonication. 15% wt/wt PEGDA LNGs contain DOPC:Chol:DSPE-PEG(2000) (80:15:5).....28

Table 3-3. Summary of PC lipid properties (courtesy Lipid Maps Structural Database and Avanti Polar Lipids).....31

Table 3-4. Summary of size and uniformity of POPC:Chol:DSPE-PEG(2000) (80:15:5) LNG patirlces (10% v/v) prepared using each extrusion technique. Standard deviation is from 3 samples explicitly made for this experiment.....37

Table 3-5. Summary of bulk phase removal data for preparation of POPC:Chol:DSPE-PEG(2000) (80:15:5) LNG particles (15% wt/wt) prepared by extrusion through a 100 nm and 80 nm nanoporous filter.. 38

Table 3-6. Encapsulation and aggregation of doxorubicin in LNG particles. Error corresponds to standard deviation.....51

ACKNOWLEDGEMENTS

I would like to thank Soo Park, You Jung Kang, Chung-Fan (Joseph) Kou, and Dr. Sheereen Majd for all the help they have provided over the past year. Thank you for making my first year of graduate school special and for inviting me into the research community.

Chapter 1

Introduction

1.1 Nanoparticle Design

Nanomedicine is the application of nano-scale materials to enhance or alter the activity and efficacy of pharmaceuticals within a biological environment. Since its inception in the early 1970s, excitement over the opportunities nanomedicine could provide to various fields of medicine has led to a plethora of publications and 200 plus products in pre-clinical trials[1]. Early forms of nanomedicine took the form of liposomal nanoparticles, or self-assembled spherical lipid-bilayers, used to encapsulate bioactive molecules. Polymeric and metallic nanoparticles quickly followed after giving rise to large volume of literature and approximately 200 products in clinical and preclinical trials[1]. Success in the clinical and industrial realm has however been daunted by difficulties in data interpretation and an overall lack of understanding of fundamental nanoparticle design. These shortcomings are best illustrated by the underwhelming success of Doxil, a liposomal doxorubicin blend, for the treatment of ovarian cancer. Doxil achieved astounding success in preclinical trials but, alongside other liposome blends, failed to show significant improvements in clinical trials and subsequent large-scale usage over the non-encapsulated doxorubicin therapy[2,3]. At best, slight advances in overall toxicity were accomplished at the cost of shifting toxicity away from major organs to the skin and feet[2–4]. The large discrepancies between the preclinical data and the clinical results have caused many researchers to retrace back to fundamental design principles[5,6]. This chapter aims to discuss some of the lessons learned from early nanoparticle formulations and advances in nanoparticle design.

1.1.1 Size and Shape

Size has been one of the most studied aspects of nanoparticle design in recent decades. It is difficult, however, to separate these studies from those on the shape of the particle. These parameters are fundamentally linked to each other in the presentation of the nanoparticle both to the biological environment and to the surface of cells. Therefore, it is important to develop a physical basis as to how these factors relate to observed phenomenon. This section aims to highlight how previous studies have interpreted the influence of size and shape on nanoparticle behavior.

1.1.1.1 Nanoparticle Accumulation and Blood Circulation

Particulates of any size or shape within vasculature naturally disturb the fluidic environment. The influence of shape and size can easily be seen in the observed differences between red blood cells (RBCs) and white blood cells (WBCs) in blood flow[7,8]. RBCs are small, bi-concave discs that align with the flow of the vascular network depending on the ratio of the inertial forces to the viscous forces. The ratio of the aforementioned forces is commonly reported as the Reynold's number. In high inertial regions of the vasculature, such as the aorta, RBCs align with the flow and take on a torpedo morphology. In contrast, in low Reynolds number flows RBCs align perpendicular to the flow and are usually forced to squeeze through the capillary space. In contrast, WBCs are spherical cells with excess membrane folds that roll along the edge of all vascular networks where they come into contact with endothelial cells. The shape of both RBCs and WBCs is the primary reason that these cells interact with vascular flow differently and allows each cell type to carry out their specific functions.

Similarly, nanoparticle morphology plays a significant role in the fluidic stability experienced by particles within the body. For instance, Dr. Hai-Quan Mao's lab at John Hopkins fabricated a plasmid-templated chitosan nanoparticle system in which the nanoparticle had a vastly different morphology based upon the solution environment used during the fabrication procedure[9,10]. When examined *in vivo*, particle morphology had a significant impact on the final tumor and liver accumulation concentration (Figure 1.1). The primary hypothesis offered by Dr. Mao's group is that the elongated dimension of the worm-like shape of the plasmid particles was the reason these particles had reduced clearance, due to decreased interaction with immune cells by remaining suspended in the fluid similar to RBCs in high Reynolds flow.

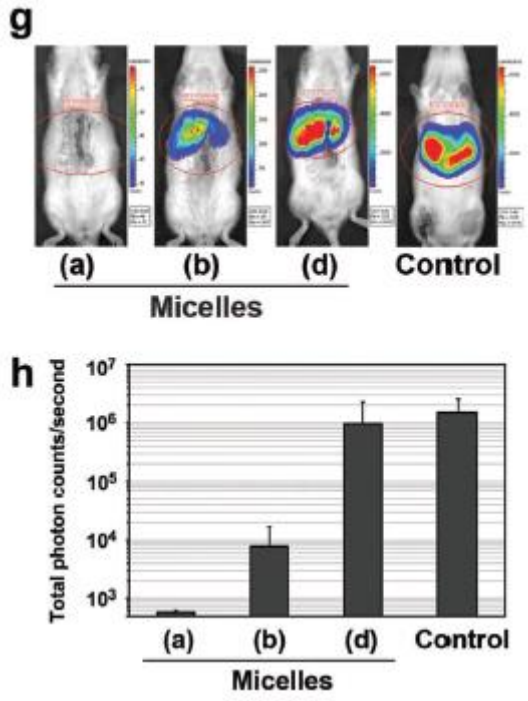

Figure 1-1.) *In vivo* data demonstrating the importance of fluidic stability of nanoparticles g.)Increasing elongation of the worm-like micelles (increases left to right) increased fluorescent accumulation at the tumor site. h.) Corresponding photon counts at the tumor site as a quantifiable measurement of concentration. Figure adapted from Jiang et al[9]

To date, the enhanced permeation and retention (EPR) effect in tumors has been the primary means of targeting for the majority of FDA approved nanomedicines[2–4,11]. Cancerous

cells produce large quantities of vascular endothelial growth factor without proper control to increase angiogenesis[11]. Fortunately for nanoparticle targeting, these large fenestrations in the vasculature cause the particulate content of the blood to accumulate at the tumor site[11,12]. Nanoparticles that are between the size of 20-200 nm are able to take advantage of this effect by avoiding clearance by the kidneys and liver prolonging overall circulation[11–13]. Shape also plays a role in prolonging circulation by providing energetic challenges for protein adsorption. The protein corona that develops around nanoparticles is theorized to control the cellular recognition of nanoparticles[14–16]. Protein adsorption is a reversible process that is kinetically and thermodynamically controlled[15]. Controlling the shape is one possibility to shift the adsorption in favor of a kinetically favored corona or an energetically favored corona based upon the surface energies for displacing adsorbed water molecules.

1.1.1.2 Tissue Penetration and Cellular Uptake

Nanoparticle size also has been shown to have an impact on tissue penetration. For intravenous administration of nanomedicines, the endothelial cell lining of the vasculature can have large impacts on the tissue distribution of nanoparticles. The blood brain barrier is a classic example of how barriers can be a hindrance in the administration of pharmaceutical therapies[12,17–19]. Size has shown to have an influence on the ability of nanoparticles to bind and cross the blood brain barrier as well as penetrate into solid tumors. In general, smaller particles penetrate deeper into tissues[6,12]. Deeper tissue penetration however usually comes at the cost of shorter dwell times within tumors[5,12]. As was mentioned earlier, a clear example of this is the size dependence for liver and kidney clearance. Nanoparticles smaller than 20 nm are quickly removed in the Kidneys while nanoparticles larger than 200 nm accumulate in the macrophages of the liver and

spleen[6,11,12]. Particles larger than 200 nm also accumulate in the lungs prompting some to propose size as a possible targeting mechanism for lung diseases[20].

The size and shape of a nanoparticle also have dramatic influences on the recognition and uptake when contacted by cells. One of the primary hindrances to nanoparticle targeting is the mononuclear phagocytotic system (MPS). Monocytes and its derivative cells, specifically macrophages, are professional phagocytotic cells that engulf extracellular material for presentation to the adaptive immune system[3,21,22]. Nanoparticles are prime targets for the MPS cells and often accumulate in macrophages. As has been noted in numerous studies and reviews, properties that make nanoparticles uniquely identifiable within the blood circulation often result in increased macrophage uptake[6,12,21,23,24].

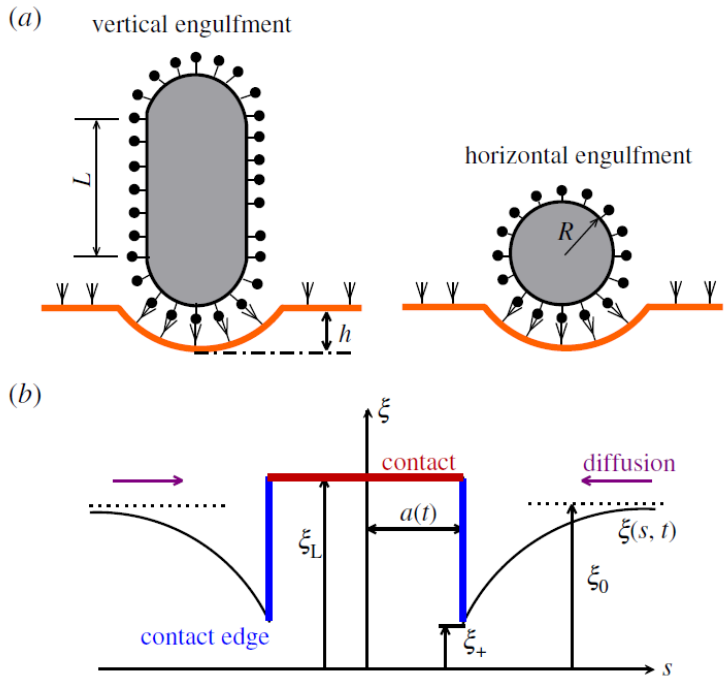

Figure 1-2.) Functional schematic of shape-dependent activation of membrane bound receptors a.) A depiction of the functional dimension, length (right) or radius (left), that corresponds to activation of receptors on the membrane as the receptor is engulfed by the cell. b.) A concentration gradient depiction of receptor activation and diffusion at the site of nanoparticle contact. Figure adapted from Wang et al.[25]

Unfortunately, many of the properties that increase MPS uptake are also the properties that influence normal cellular uptake (Figure 1-2). Size influences nanoparticle uptake into the cellular environment by controlling receptor activation, membrane depletion, and the thermodynamic barrier to endocytosis[12,19,26–31]. As the receptors diffuse down the concentration gradient to points of nanoparticle contact, the limiting activation energy is quickly met given a sufficient particle receptor density. In general, the total accumulation within a cell of particles greater than 50 nm in size is not limited by receptor activation but instead by membrane depletion[6,25]. However, from a kinetic perspective nanoparticles that are spherical or ellipsoidal/rod-like have been shown to achieve the fastest uptake depending on the size of the particle[6,12,26]. These results confirm some of behavior exhibited by viruses, which naturally change their size and shape to exploit endocytosis[9,32]. It is important to note that the majority of nanoparticle uptake research has been performed on immortalized cell lines, macrophages, and cancerous cells. Each of these cell types are already known to have increased uptake compared to classical somatic cells[23,33]. The *in vivo* environment is also highly complex and not easily understood. A simple example is the difference between *in vitro* and *in vivo* uptake of Doxil. By controlling lipid content and size, Doxil was fabricated to have preferential uptake by ovarian tumor cells. After large-scale usage however, it was proposed that Doxil merely accumulates at the tumor site rather than by uptake of the tumor cells[2]. It is therefore important to consider that nanoparticle uptake is not a simple function of size and shape.

1.1.2 Surface Charge and Stability

Surface charge and zeta potential are the oldest measured properties of nanoparticles dating back to the earliest liposome formulations. It is important to clarify the primary difference between these two measurements and the difficulty in achieving an accurate measurement. The

surface charge of a nanoparticle is the charge directly on the interface between the polymer/metal/phospholipid head and the external environment. In contrast, zeta potential is the measurement of the electrical potential with respect to the particle's hydrodynamic diameter. For this reason, zeta potential measurements are often of a lower magnitude that the surface charge measurements of nanoparticles[2]. Whenever the difference of the hydrodynamic radius and the physical diameter of the nanoparticle exceeds the Debye length of the particle in physiological solution the value of the zeta potential will be drastically different than the surface charge. Unfortunately, few publications make a distinction between these two properties as measuring the surface charge is often difficult. Therefore, unless otherwise noted surface charge in the preceding sections is referring to the zeta potential, or the charge at the point of hydrodynamic interaction. The aim of this section is to present the influence of electrostatic interactions upon nanoparticle behavior *in vitro* and *in vivo*.

1.1.2.1 Circulation and Cellular Uptake

The vast majority of nanoparticle formulations have sought to either have a negative or neutral charge[12,16,19,24,34]. Neutral nanoparticles have often been reported to have the longest circulation time, which allows these particles to take advantage of the EPR effect[3,11,19]. Negatively charged particles also have relatively long circulation times due to repulsive interactions with the abundant negatively charged blood protein[14,19]. Positively charged particles are limited mostly to gene therapies due to dramatic increases in toxicity when used in both *in vitro* cultures and in *in vivo* animal models. The toxicity of positively charged particles is theorized to be a result of electrostatic membrane binding and subsequent destabilization[19,35,36].

Zeta potential has been identified to be a primary contributor to cellular uptake rate, overall accumulation, and endocytotic route. An overview of the endocytotic routes are provided

in Figure 1-3. Positively charged particles appear to recruit non-clathrin mediated endocytosis mechanisms while negatively charged and neutral particles appear to enter cells according to the clathrin route[34,36,37]. Negatively charged particles have also been shown to induce macropinocytosis in MPS cells which is theorized to occur due to disruption of lipid fluidity[34,38]. Overall, positively charged particles display the greatest total accumulation[19]. The positive charge however needs to be masked to avoid rapid clearance by the MPS an off-site toxicity. An interesting application of surface charge in endocytosis was discovered when analyzing the intracellular trafficking of nanoparticles capable of switching charge due to protonation. For example, PLGA switches charge according to the pK_A of its acid functional groups. In the highly acidic environment of the late endosome/ early lysosome PLGA particles become positively charged and disrupt the endosomal stability enabling their escape into the cytosol. This phenomenon is typically referred to as the proton sponge effect and has inspired pH sensitive swelling and release from nanoparticles[39–42].

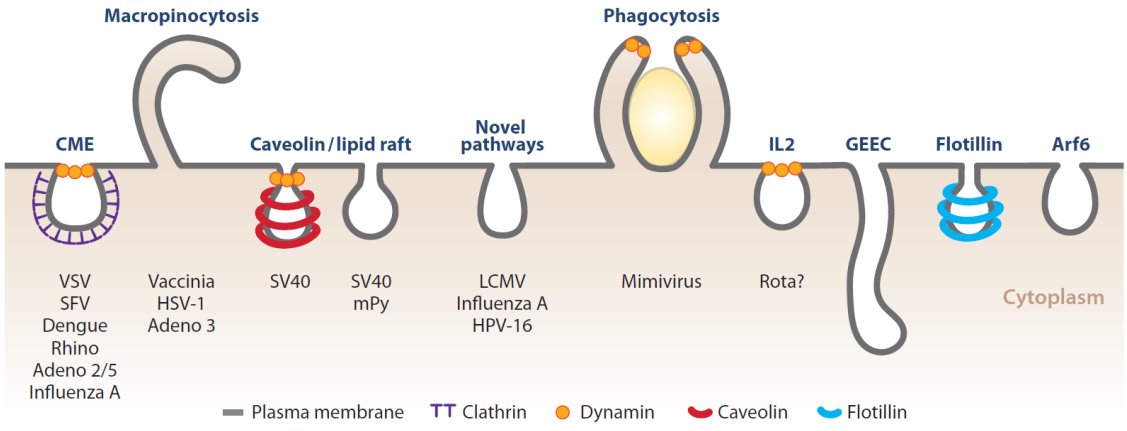

Figure 1-3.) An overview of the known endocytosis routes of entry into the intracellular space. Figure adapted from Mercer et al.[43]

One of the most important aspects of surface charge is the generation of the protein corona in biological fluids. Upon entering the biological medium, nanoparticles are forced to interact with hundreds of proteins with relative charges and affinities for the nanoparticle surface. Proteins bind to charged nanoparticles to shield the particle's charge, commonly bringing nearly all nanoparticles to a negative charge. The early and intermediate compositions of the protein corona are strongly dependent on the strong electrostatic interactions that occur with the surface of the nanoparticle[14]. There is some debate whether or not protein adsorption should be encouraged and controlled using interactions such as electrostatics, or avoided using hydrophilic coronas such as polyethylene glycol (PEG)-chains.

1.1.2.2 Stealth Coronas and PEGylated Nanopartricles

PEGylation is a common strategy employed by nanoparticle fabrications to improve circulation half-life and immune evasion. The end result of adding PEG chains to the outer surface of the nanoparticle is the creation of a hydrophilic shell on the outside of the particle, which decreases protein adsorption and consequently immune recognition[2,44,45]. In practice, PEGylation *in vivo* has provided longer blood circulation times and greater tumor accumulation due to the EPR effect[2,45,46]. However, these benefits come at the price of toxicity in the extremities[2,47]. Although PEGylation decreases protein adsorption and immune recognition, 'stealth' nanoparticles are not truly invisible to the immune system. Protein coronas do form around PEGylated liposomes and PEG antibodies have been found in patients given PEGylated liposomal doxorubicin over-time[47]. PEG also increases the hydrodynamic diameter of nanoparticles and provide steric hindrances to other interactions with colloids. Many researchers have included PEG in co-polymers to improve colloidal stability while also taking advantage of the hydrophilic stabilization that occurs due to PEG's ordering of the hydration shell[48,49].

For liposomal based nanoparticles, like the one discussed in this thesis, PEG is commonly added to the lipid bilayer by conjugation to the head group through a phosphodiester bond. It is important to note that this interaction commonly gives PEGylated liposomes a negative surface potential that is not necessarily reflected in the zeta potential measurement[2,47]. It is not clear whether or not this discrepancy is important, but it is important to note that PEGylation does not neutralize surface charge. PEGylation however may make it difficult for nanoparticle interactions to occur within the Debye length of the surface charge.

1.1.3 Elastic Toughness

The elastic toughness is defined as the relationship between stress and strain within a given dimensionality. Elasticity is commonly represented by the Young's modulus, also known as the elastic modulus, which is the linear slope constant relating the stress to the strain. As is common in polymer studies, the elastic modulus varies significantly with the strain rate signifying the viscoelastic nature of nearly all materials. Mechanical properties in general have been poorly investigated in the nanoparticle field primarily due to an inability to properly measure many of these properties. Theoretical work and computational models however have predicted a significant impact from these properties[25,28,29,32,50–52]. With recent advents in atomic force microscopy and optical microscopic techniques, these properties can now be experimentally evaluated to confirm or reject the proposed theoretical implications of mechanical compliance. This section aims to highlight recent studies in the influence of elastic properties on nanoparticle efficacy *in vitro* and *in vivo*.

1.1.3.1 Circulation and Cellular Uptake

Elasticity so far has been shown to have an influence on nanoparticle endocytosis and biodistribution. As is depicted in Figure 1-4, elasticity was shown to have an influence on the overall uptake exhibited by particular endocytosis mechanisms[23]. Specifically, stiff particles preferred uptake by clathrin-dependent processes while soft nanoparticles favored micropinocytosis. Intermediate moduli nanoparticles, here in the range of 30-130 kPa favored uptake by caveolae-mediated processes. These results may indicate that the energetic costs of one endocytosis mechanism over another differ significantly. It is, however, important to note that theoretical work has indicated that it is the ratio of the elastic moduli between the cell and the nanoparticle that govern the thermodynamic costs of endocytosis rather than simply the nanoparticle alone[25,28].

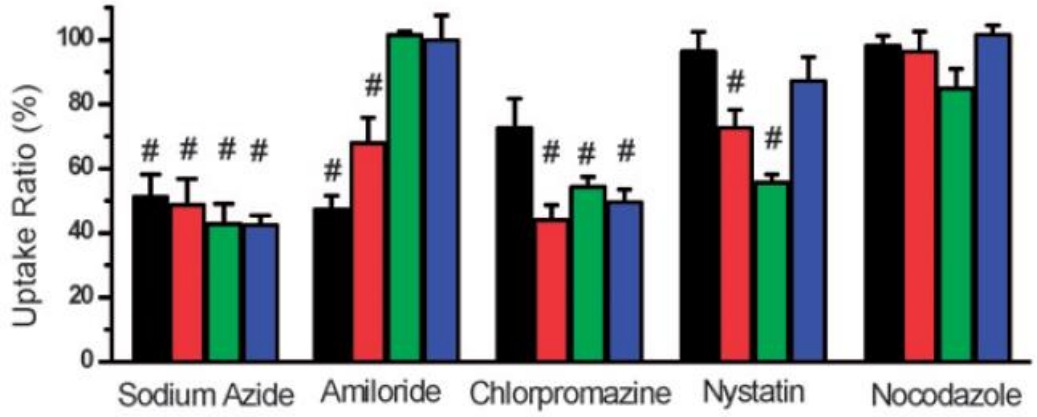

Figure 1-4.) Inhibitor study of the influence of elasticity of nanogels on endocytosis mechanism. Bars left to right show increasing elasticity (20-200 kPa). Uptake in the presence of the identified inhibitor is presented as a percentage of the uptake of each particular particle formulation in standard medium. Sodium azide was used as an inhibitor for ATP-dependent endocytosis, amiloride was used as an inhibitor of micropinocytosis, chloropromazine was used as an inhibitor of clathrin-mediated endocytosis, nystatin was used as an inhibitor of cavaeloe mediated endocytosis, and nocodazole was used as an inhibitor of microtubule-associated endocytosis. Figure adapted from Banquay et al.[23]

Dr. Mitragotri's research group was also able to show that the mechanical properties of hydrogels influenced the distribution of the nanoparticles *in vivo*[53]. Stiff nanoparticles (3000 kPa)

were rapidly cleared from the circulation of mice while soft nanoparticles (10 kPa) were able to persist for much longer dwell times. When they used cell lines to investigate the possible mechanism, they discovered that stiff nanoparticles underwent endocytosis by all cell types faster and accentuated the influence of targeting ligands. Therefore, the clearance of the stiff nanoparticles *in vitro* is a likely confirmation that the MPS readily recognizes and removes the colloids from the blood by phagocytosis. This finding fits particularly well with another publication, which found that macrophages uptake nanoparticles of greater than 200 kPa at high rates[54]. Overall, these publications present an interesting paradigm in nanoparticle design in that high cellular uptake rate is undesirable due to immune clearance. Reducing the elastic toughness of particles may therefore be an attractive option to reduce nanoparticle clearance without the addition of large macromolecular moieties onto the surface of the nanoparticle.

1.1.4 Targeting Schemes and Controlled Release

One of the primary aims of nanomedicine is control the activity of molecular agents to particular tissues or cellular compartments. Specific control over this activity allows for improved reduced toxicity and improved therapeutic efficacy. There are three main methods that have been employed to date to take advantage of specific pathological phenomenon: i.) increased vascular retention (i.e. usually taking advantage of the EPR effect), ii.) surface protein expression, and iii.) localized signals within the target tissue. These targeting schemes have been referred to as passive targeting, active targeting, and environmental sensitivity by members of the nanomedicine community. This section aims to highlight historical methods and recent advances in controlled molecular efflux from nanoparticles.

1.1.4.1 Passive Targeting

Passive targeting looks to take advantage of changes in the vascular environment near or at the target tissue. For this reason, passive targeting is commonly employed to target tissues that have large metabolic demands or directly interface with circulating blood. The classical example of this form of targeting is delivery to solid tumors through the EPR effect[11,13]. The EPR effect was already discussed earlier in the section "Size and Shape". Other examples of passive targeting include targeting to the clearance systems that normally plague other drug delivery systems. Delivery to the liver, kidneys, and lung are in particular susceptible to this targeting scheme[3,20]. Other examples include nanoparticles that selectively activate or sediment in high shear environments, or areas with poor lymphatic clearance[55]. Shear-activated nanoparticles are commonly employed for selectively treating occluded vessels to take advantage of the change in the fluidic regime.

The best way to take advantage of passive targeting is to limit clearance from off-site systems. Classically, the best way to improve circulation half-life has been the development of hydrophilic polymer coronas to reduce protein adsorption[45,55]. The theory behind this method is that the biological fluid can only interact and eliminate colloidal species, or any biomaterial, that has protein adsorbed to its surface. However, passive "stealth" techniques have proven to be less beneficial than hoped. It has become clear that the body is capable of developing antibodies for recognition of nearly any entity, including the polymer coating PEG[47]. EPR accumulation at tumor sites also rarely accounts for more than 10% of the administered dosage of nanoparticles[2,5,11,12]. Passive targeting is also difficult to apply to tissues that are protected by endothelial cells[3,5,56]. In this case, nanoparticles must first adsorb to the endothelial cell lining and pass either between or through the barrier prior to reaching the target.

1.1.4.2 Active Targeting

Unlike passive targeting, active targeting relies on the chemical specificity of protein binding by attaching ligands to the nanoparticle surface. The coated ligands then interact with the biological environment in a predictable fashion. Targeting ligands are usually chosen to meet either a specificity criteria or a therapeutic criteria. When a targeting ligand is chosen for specificity, ideally the receptor antigen is significantly present within the target tissue. A powerful example of this technique is its use in targeting inflammation markers expressed on the surface of vascular endothelial cells[57–59]. Nanoparticles in the vasculature accumulate at sites of injury using this method by binding cell markers similar to the binding of white blood cells to the vessel wall. Other examples of specificity binding include targeting of the over-expressed tumor-associated antigens. A classic example of an over-expressed tumor-associated antigen is the folate receptor, which is discussed more below[60–62].

Targeting the folate receptor also revealed an added therapeutic nuance of antigen-targeting. Nanoparticles that targeted the folate receptor were able to overcome multidrug resistance due to changes in drug internalization mechanisms[60,61]. In fact, numerous other drugs have been reported to have altered activity when encapsulated or conjugated to a nanocarrier[5,6]. The differences in drug activity highlight the main advantage of active targeting: the provision of a thermodynamic driving force for endocytosis[28,63]. Changes in the free energy of adsorption and protein cascade activation allow ligand-coated nanoparticles to be internalized at significantly enhanced rates[53,64]. Active targeting that takes advantage of similar phenomenon are chosen to confer an added functionality to the nanoparticle. Another example of added functionality is when the nanoparticle ligand is also the therapeutic agent. Immunomodulation is a recent form of ligand-mediated therapeutic activation[65–68]. Rather than induce cell death, nanoparticles chosen for immunomodulation attempt to activate quiescent immune cells, to present an antigen to

macrophage and professional antigen-presenting cell network for an adaptive immune response, or mediate the inflammatory response.

Active targeting is not without its drawbacks. Ligands on the surface of the nanoparticle are chosen to interact with specific targets but an unfortunate consequence is protein adsorption and immune recognition are naturally enhanced in this situation[63,64]. Unless used to target immune cells, active targeting commonly enhances clearance by MPS cells. Nanoparticles that take advantage of the EPR effect have been shown to have less accumulation at the tumor site when combined with targeting ligands for this reason[6,69]. Targeting ligands also change the surface chemistry of the nanoparticle, altering the degree of hydrophobicity and surface charge. One method to avoid these changes is to attach the targeting ligand at the end of a hydrophilic polymer linker[70]. However, increased PEG density, even when ligands are attached to the end of the polymer chain, decrease specificity and accumulation[71]. It should be noted that changes in the zeta potential due to PEG shells or proteins at the end of polymer chains do not necessarily correlate to actual surface properties of nanoparticles.

1.1.4.3 Environmental Sensitivity

In recent years, researchers have moved towards environmental cues and external signals as a means to control the release of the bioactive payload of nanoparticles. Environmental and signal sensitive nanoparticle formulations present the unique opportunity to dynamically change physicochemical properties in response to disease pathology or clinician input. The pH responsive nanoparticle was one of the first environmentally responsive hydrogels designed for both sensitivity to the tumor microenvironment and to take advantage of the proton sponge effect mentioned previously[41,72–74]. Other examples of stimulus sensitivity include ionic strength[74], temperature[75–77], oxidation and reduction[78], magnetism[62,79,80], and light[81,82]. Liposome

formulations can also be sensitive to ultrasound for targeted delivery[83]. Ultrasound, magnetism, light, and temperature are all interesting stimuli as the signal can be generated at the target tissue site by clinicians.

Many environmentally sensitive nanoparticle fabrications have either been liposomes or nanogels, nanoscale hydrogel particles. Hydrogel polymers are uniquely accessible for biomedical applications as they are both hydrophilic and do not present diffusional barriers[84]. Nanogels can also be made sensitive to a number of stimuli[85]. Other examples of controlled release in response to stimulus include biomacromolecules such as nucleic acids[86] or proteins/polypeptides[77]. The chemistry of biomacromolecules offer precise control over nanoparticle properties however they often are difficult to produce and expensive. Fortunately, many of these materials can be combined for the development of robust nanoparticle control. Hydrogels are perfect for encapsulation of biomacromolecules and can be formed inside liposomes[75,87–89]. Together, these features make for an interesting design choice for precise control over a multitude of physicochemical properties.

1.2 Project Goals and Hypotheses

The main goal of this project was to expand upon the potential of hydrogel-filled nanoliposomes for drug delivery purposes. We hypothesized that the addition of a hydrogel core to traditional nanoliposomes would improve the stability of these nanocarriers and provide control over the release properties. To test this hypothesis, we adapted a liposome template technique, depicted in Figure 1-5, to develop a highly versatile fabrication system. We will refer to these nanoparticle vesicles as “liposome nanogels” (LNGs). In order to compare our findings with previous results, we chose to use the pre-polymer polyethylene glycol diacrylate (PEGDA). PEGDA is an established biomedical polymer with a small molecular weight (575 MN) and

sensitivity to radical polymerization when catalyzed by the photoinitiator 2-hydroxy-2-methylpropiophenone[84,90,91]. PEGDA's hydrophilicity is known to have little impact on the diffusion of small molecules. Therefore, we hypothesized that the main advantage of the hydrogel core would come from stabilization of macromolecular structures and an ability to resist deformation. As mentioned earlier, liposomes are often reported to have low stability *in vivo*[2,47]. The low stability is often attributed to sudden rupture during the injection process. To determine whether or not nanogels were more resistant to rupture when compared to liposomes, we subjected the nanoparticle formulation to harsh detergents and constant stirring in biomimetic environments and compared the results to liposome literature. We predicted that the nanogel core would provide resistance to liposome rupture by mechanically stabilizing the liposomes against harsh fluidic environments and preventing detergent pore formation from collapsing the membrane.

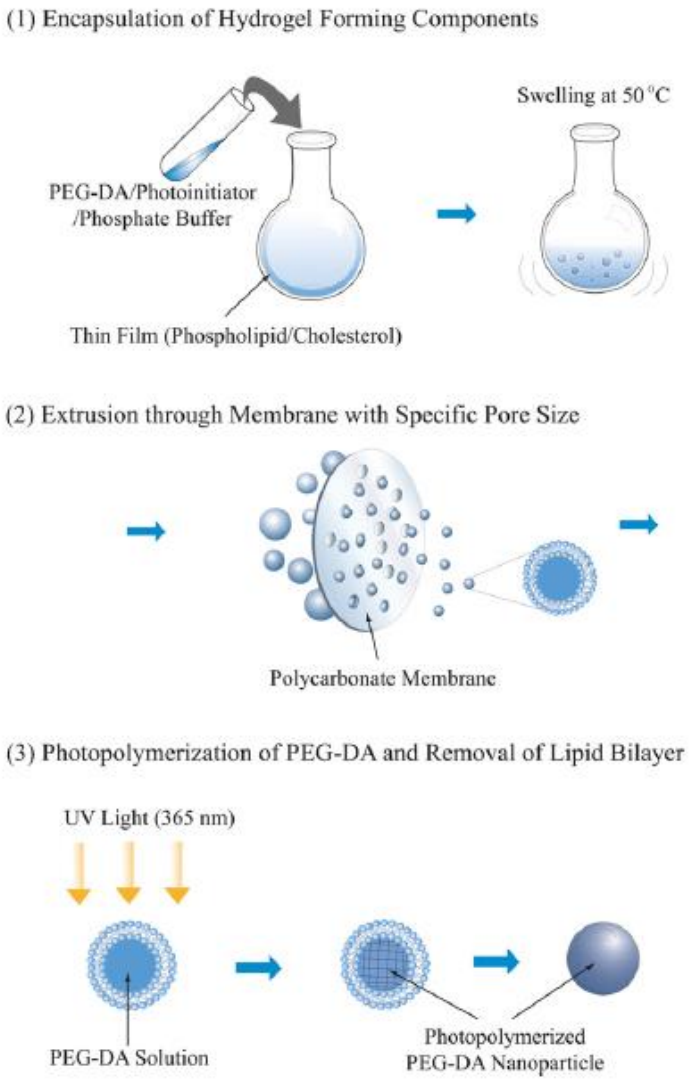

Figure 1-5.) Schematic demonstration of selective gelation of hydrogels within a liposome template. The process is broken down three steps: (1) hydration of a lipid film with polymer solution, (2) sizing of the liposomes using extrusion, (3) and selective gelation using UV in the interior of the liposome. Figure adapted from An et al.[88]

In order to evaluate the influence of the polymerized hydrogel core on drug encapsulation and diffusion, we examined these properties in the context of the small hydrophilic molecule rhodamine123 and the common liposome drug doxorubicin. To assess if encapsulation of hydrophilic small molecules was perturbed by the presence of pre-polymer in solution, we added rhodamine123 to the hydration solution and monitored its fluorescence in liposomes that had polymerized cores as well as liposomes without polymer in solution. Doxorubicin, a common

anthracycline for the treatment of a wide-range of cancers, was chosen to demonstrate active loading using a sulfate gradient method as well as stabilization of a macromolecular structure. The ammonium sulfate gradient, established by hydrating liposomes with a sulfate salt solution and subsequently replacing the bulk solution with isosmotic salt, allows for encapsulation of nearly 100% of doxorubicin added to the solution up to a saturation point of 0.2 mg/mg doxorubicin/phosphatidyle choline[92–94]. Once inside the liposome, doxorubicin is known to self-aggregate creating a stable doxorubicin crystal[2,47], after which the disassociation of the crystal is required for doxorubicin to exit the nanoparticle. We hypothesized that the addition of hydrogel to the liposome interior would protect the doxorubicin crystal and prevent disassociation and subsequent efflux into the bulk solution by diffusion of the aqueous solute down the concentration gradient.

Chapter 2

Experimental Methods and Materials

2.1 Materials

Polyethylene glycol diacrylate (PEGDA, 545 Mn), 2-hydroxy-2-methylpropiophenone, a phosphatidyl choline assay kit, sodium citrate dihydrate, and citric acid were all purchased from Sigma-Aldrich. Sodium chloride and dialysis tubing (3500 MWCO) were purchased from Fischer Scientific. Palmitoyl oleyl phosphatidyl choline (POPC), dioleyl phosphatidyl choline (DOPC), cholesterol, lissamine rhodamine-tagged disteroyl phosphatidyl choline (Rho-DSPE), disteroyl phosphatidyl choline PEG 2000 (DSPE-PEG), and a mini-extruder set were all purchased from Avanti Polar Lipids. 200, 100, and 80 nm polycarbonate extrusion filters were purchased from Whatman. Fetal bovine serum (FBS) was purchased from Atlanta Biologics. Ammonium sulfate was purchased from BDH. PBS tablets were purchased from Amresco. Sephandex G-25M was purchased from GE Healthcare.

2.2 Fabrication of Lipid Coated Nanogels

Liposome nanogels (LNGs) were fabricated by adapting the liposome bioreactor technique detailed in previous publications[48,88,95]. The following sections provide an overview of this technique as well as the changes we made to the fabrication procedure.

2.2.1 Formation and Sizing of Liposomes

Multilamellar vesicles (MLVs) were prepared by first drying a chloroform-lipid solution of PC (either DOPC or POPC), cholesterol, and DSPE-PEG at a molar ratio of 4:1:0.25. Rho-DSPE was included at 1% mol for fluorescent studies. Final liposome solutions had a PC concentration of 3 mM. After drying the lipid film in a rotary vacuum pump, lipid films were hydrated with a pre-polymer solution containing PEGDA at various concentrations (10% or 50% v/v, 15% w/v for drug-entrapment studies) and 2-hydroxy-2-methylpropiophenone (0.1% v/v; referred to as photoinitiator) by vortexing the solution 5 times for 30 seconds each. Rhodamine 123 (50 nM) was included in the pre-polymer solution to visualize encapsulation during the hydration step. Samples with PEG concentrations 50% (v/v) were sonicated 4 times for 2 minutes each with 1 minute between each interval. The MLV solution was then sized to form small unilamellar vesicles (SUVs) of size ~80 nm by extruding the sample either stepwise through a 100 nm and 80 nm pore size polycarbonate filter for 11 passes each, or through a 100 nm and 80 nm pore size filter set stacked together for 11 passes total.

2.2.2 Removal of Bulk Phase Photo initiator

Photoinitiator contained outside the intraliposomal space was removed from the solution by one of three methods: dialysis against a large volume of isosmotic solution (100x sample volume), dilution by increasing the volume of the solution 5x with deionized water or 1X PBS, or by performing a buffer exchange in a Sephandex G-25M column with 1X PBS or an isosmotic solution of sodium chloride or sodium citrate. After removing the bulk phase photoinitiator, a hand-held 100 W UV lamp was used to polymerize the particles through direct exposure for 5 minutes. All samples were then stored at 4˚C for later use.

2.2.3 Phosphatidyl Choline (PC) Assay

After removing the bulk phase photo initiator, 1 µL of the SUV solution was suspended in 99 µLs of isosmotic solution (typically 0.15 M sodium chloride). A PC assay kit purchased from Sigma was then used to analyze the phosphate content of the solution after enzymatic hydrolysis. For this reason, care was taken that no phosphate was introduced to the system prior to the assay. The fluorescence of the phosphate solution was then analyzed by exciting the solution at 535 nm and recording the fluorescence at 587 nm. The recorded intensity was then determined via a calibration plot made with PC standards.

2.2.4 Ammonium Sulfate Gradient for Loading Doxorubicin

Ammonium sulfate was used to create a stable pH gradient between the intra and extra liposomal spaces. The intraliposomal space was made to have a sulfate concentration of 155 mM by adding the ammonium sulfate salt to the pre-polymer solution prior to the hydration of the lipid film. We then established a stable gradient by replacing the extraliposomal buffer with 0.15 M NaCl or 0.123 mM sodium citrate Sephandex G-25M columns. The column buffer exchange was used in the establishment of the gradient as it was deemed to be the most convenient and reliable method for removing bulk photoinitiator. Doxorubicin HCl, stored in deionized water at a concentration of 10 mg/mL, was then added into the SUV solution post-buffer exchange and incubated for a variable amount of time at a ratio of 0.2 mg/mg PC. We then used another Sephandex G-25M column to remove the excess doxorubicin and terminate the incubation period by exchanging the doxorubicin solution with 1X PBS. The final SUV solution was then immediately irradiated with UV for 5 minutes to polymerize the hydrogel solution inside the lipid space. All samples were then stored at 4˚C for later use.

2.3 Nanoparticle Characterization

2.3.1 Size and Zeta Potential

A Malvern Zetasizer from the Materials Characterization Lab of the Materials Research Institute was used to determine the size distribution of the final LNG solutions by dynamic light scattering (DLS). Briefly, 1 mL of solution was placed in a cuvette and a beam is shone through the sample. An auto-correlation curve is fit to the intensity of the light beam to determine the diffusion of the nanoparticles through the focal volume of the beam. The decay of the auto-correlation curve is then related to the size of the particle through the Einstein-Stokes relationship. A similar procedure is used to determine the zeta potential of the particles. Light is scattered by the particles while being exposed to alternating electrical fields determine the influence of the field potential on the decay of the auto-correlation function. The Henry equation can then be used to determine the zeta potential.

2.3.2 Morphology

Scanning Electron Microscopy (SEM) and cryogenic transition electron microscopy (Cryo-TEM) were used to evaluate the morphology of particles in a de-hydrated and hydrated environment. Both machines were made available by the Materials Characterization Laboratory of the Materials Research Institute. To prepare samples for SEM, we placed a drop of LNG solution on a glass coverslip to dry prior to imaging. The process of drying destroys the structural integrity of the liposomes causing the hydrogel core to disassociate from the lipid bilayer. Samples were then sputter coated with a thin layer of Iridium immediately prior to imaging to improve the sample conductivity. Cryo-TEM samples were prepared by placing the sample on a

carbon grid and plunging the grid into liquid ethane to encase the sample in vitreous ice. Low-electron dose TEM images were then taken to preserve the ice.

2.3.3 Stability in Biomimetic Environments

The stability of LNG solutions, without encapsulated doxorubicin, were evaluated in aqueous and protein environments by suspending 0.1 mL LNG solution in 0.9 mL deionized water or an equal volume of FBS solution respectively. The resulting LNG solution was then measured each day for a week using DLS. Surface charge could not be measured due to low phase signal and the disruption of the signal from the serum.

2.4 Doxorubicin Encapsulation and Release

2.4.1 Encapsulation Efficiency and Doxorubicin Gelation

Doxorubicin was encapsulated inside of the LNG system as previously mentioned[2,47,94]. 0.1 mL of the final LNG solution, post-polymerization if analyzing the benefits of an entangled nanogel core, were then evaluated using a multiplate reader (Flexstation 3R, Molecular Devices) for absorbance at 470 nm, 492 nm, and 550 nm. The 492 nm peak was used to evaluate the total doxorubicin content[17,96] based off a calibration curve generated using doxorubicin and PBS. Doxorubicin gelation was evaluated by recording the ratio of the 470 nm absorbance to the 550 nm absorbance that occurs when the drug forms a complex with the sulfate ions and self-aggregates[94].

We also conducted an analysis of the doxorubicin encapsulation kinetics by observing the fluorescent decay of doxorubicin as it entered the liposome core[94]. The kinetics assay was

performed by filling 6 wells in a 96 well plate with SUV solution with an established sulfate gradient. Doxorubicin was then added to SUV solution at a ratio 0.2 mg/mg PC. This 1:5 mg ratio of doxorubicin and PC are the established theoretical maximum concentrations that occur using the sulfate loading technique[2,47,94]. The fluorescent intensity decay of the solution at an excitation of 480 nm and an emission of 570 nm were recorded over 6 hrs. A plot of the decay was made versus the photobleaching that occurred in 0.1 mL doxorubicin PBS solution over the same period of time. An association constant for doxorubicin to the sulfate ion was then determined by fitting the data with a linear regression.

2.4.2 Release Profile

We evaluated the release of doxorubicin from the fabricated LNG and SUV solutions by preparing 3 mL of final solution and incubating it in 3 L of 1xPBS in 3500 MWCO dialysis bags. 0.1 mL of each bag was removed at several time points (1, 2, 4, 6, 12, 24, 48, 72, 96, 120, 144, 168 hrs) for absorbance at 492 nm. The gelation ratio between the absorbance peaks of 470 nm and 550 nm were also recorded to track the stability of the doxorubicin aggregation over release. A release plot was then created by normalizing the absorbance data against the starting absorbance of each solution.

2.4.3 Statistics and Significance

All values were calculated as the mean of 3 samples unless otherwise stated. Error bars represent the standard deviation from the mean. Statistical significance was calculated based upon an $\alpha = 0.05$ to ensure a 95% confidence interval, and is represented by an asterisk in charts and graphs.

Chapter 3

Results and Discussion

3.1 Fabrication and Characterization of LNGs

In order to prepare liposome nanogels (LNG), or hydrogel-core liposomes, we chose to use a method that has previously been described as a liposome bioreactor template. In this method, a lipid film was first hydrated with solution containing polymer pre-cursors alongside polymerization catalysts. For this study, we chose to use PEGDA, an established biomedical polymer, and 2-hydroxy-2-methylpropiophenone, a common photoinitiator that has previously been used with PEGDA. Salts or other molecular agents were also included during the hydration of the lipid film for a form of volumetrically-oriented passive loading. Following hydration, which usually involved vigorously vortexing the liposome solution, the liposomes were broken into nano-scale liposomes titanium tip sonication and/or extrusion through polycarbonate filters. The bulk photoinitiator was then removed/diluted by dialysis, dilution into a large volume of buffer, or by performing a buffer exchange in gel column allowing the SUV solution to be exposed to UV light without forming a bulk gel. The end result of this process was a uniform (PDI < 0.1) solution containing liposomes with PEGDA gel cores. We identified several key components in this fabrication on size and colloidal stability of the nanoparticles that will be discussed in the preceding sections.

3.1.1 Varying the PEGDA Content

The PEGDA content of the intraliposomal space was altered by controlling the volume fraction and the weight fraction of the polymer in the pre-polymer hydration solution. Both methods of control are considered separately below.

3.1.1.1 Volume Fraction of PEGDA

The earliest intent of this project was to develop nanoparticles with varying hydrogel densities. To this end, we proposed that by altering the PEGDA volume concentration we could control the degree of polymerization and thus the density of the intraliposomal gel. Fabricating LNGs by this method could, therefore, provide an additional control over the gel environment and potentially the release behavior of therapeutics, the degradation of the particle, and/or the cellular interaction that takes place when contact is made with the nanoparticle. To test this hypothesis, we chose volume fractions (v/v) of 10% PEGDA and 50% PEGDA to gain an understanding of drastically different hydration solution conditions.

Early results indicated that increasing PEGDA volume fraction drastically increased the size of the nanoparticles with some dependence on the fatty acid chain disorder of the liposome bilayer. The second aspect of the vesicle size will be discussed later when visiting the lipid content. The influence of PEGDA volume content seems fairly intuitive; increasing the polymer concentration in the aqueous environment hindered liposome shrinkage in all steps. Sonication and extrusion in particular became fairly difficult due to the viscous effects of high polymer concentrations. Sonication was determined to be crucial for obtaining vesicles smaller than ~300 nm with a 50% PEGDA volume concentration. 10% PEGDA volume concentration liposomes, however, were easily formed to the size of 114±13.5 nm (POPC) or 148±25.9 nm (DOPC) with

the inclusion of DSPE-PEG without sonication. These results are summarized in Table 3-1 and Table 3-2.

Table 3-1. Summary of POPC:Chol (85:15) vesicle fabrication data for samples prepared by extrusion and sonication. 15% wt/wt PEGDA LNGs contain POPC:Chol:DSPE-PEG(2000) (80:15:5).

	AVERAGE (NM)	**PDI**	**STD. AVG. (NM)**	**STD. PDI**
15% WT. PEGDA LNG	118	0.068	5.98	0.017
10% VOL. PEGDA LNG	139	0.112	5.13	0.024
50% VOL. PEGDA LNG	298	0.311	31.6	0.113
10% VOL. PEGYLATED POPC LNG	114	0.092	13.5	0.019

Table 3-2. Summary of DOPC:Chol (85:15) vesicle fabrication data for samples prepared by extrusion and sonication. 15% wt/wt PEGDA LNGs contain DOPC:Chol:DSPE-PEG(2000) (80:15:5).

	AVERAGE (NM)	**PDI**	**STD. AVG. (NM)**	**STD. PDI**
15% WT. PEGDA LNG	168	0.260	3.07	0.012
10% VOL. PEGDA LNG	120	0.324	26.8	0.206
50% VOL. PEGDA LNG	207	0.207	8.43	0.096
10% VOL. PEGYLATED DOPC LNG	148	0.449	25.9	0.263

The results from these experiments suggest that PEGDA provides resistance towards the formation of smaller liposomes. In this study we used a PEGDA polymer of molecular number average weight of 575 Daltons, which, by comparison, is approximately the size of a typical PC lipid molecule. The small size of the PEGDA polymer would not contribute significant steric hindrance to the formation of a stable liposome. A simple model of liposome formation is an analysis of the work required to form the liposome. The total work of the system should be proportional to the sum of the work required to break lipid-solvent interactions and the work of of forging lipid-lipid and solvent-solvent interactions. The work of cohesion between two lipid-

molecules and the work of cleaving the lipid-solvent interaction should remain constant, assuming negligible interactions between lipid and PEGDA molecules. Therefore, resistance to liposome diameters smaller than 200 nm at 50% v/v PEGDA concentrations may be due to decreases in favorable energetic contributions from water-water interactions. The PEGDA-water interactions could compete with water-water interactions at a 50% v/v concentration. Another aspect of this simple thermodynamic model could be then be related to the kinetics of liposome formation. PEGDA, while competitively blocking water-water coordination, could also be hindering the diffusion of lipid molecules. Increased diffusion time could cause the liposome to struggle to form the sub 200 nm constructs. An alternative hypothesis is that the PEGDA content at the interface of the intraliposome volume and the lipid bilayer disrupts cohesive interactions between the lipid molecules. At high concentrations of PEGDA, the difference in the partition coefficients between the lipid molecules and the PEGDA become diminished, disrupting membrane packing and solvent exclusion. The cohesive energy of the lipid membrane, represented by the surface tension at the interface, must therefore reach an equilibrium that is at a greater diameter than in lower concentrations due to decreased energetic contributions from lipid and solvent cohesion. Both theories may play a contributing role. Regardless, we hypothesize that effects in either theory would be compounded when using larger polymers pre-polymerization and suggest the use of small polymer chains for hydrating lipid films.

3.1.1.2 Weight Fraction of PEGDA

When we preceded to load doxorubicin into the SUV solutions, we chose to change the particle fabrication to use a 15% weight fraction of PEGDA during the hydration steps to enable direct comparison with previous reports on PEGDA nanogels[53,88,97]. When considering the previous volume fractions, 50% and 10% PEGDA volume concentrations corresponded to 53%

and 11% by weight (wt/wt), respectively. As anticipated, the results of the 10% PEGDA volume concentration and the 15% weight concentration were and no statistically significant differences were noticed between PEGDA LNG samples from these two experimental groups.

3.1.2 Varying the Lipid Content

A primary goal of investigating LNGs was to prove that the inclusion of a hydrogel core inside of a liposome would have synergistic improvements on stability of liposomes. Consequently, we hypothesized that this improvement would provide opportunities to use a larger diversity of lipids in the liposome formulations. As mentioned earlier, Doxil formulations use high transition temperature (T_g) PC lipids in order to prevent leakage of doxorubicin. These PC lipids however have little *in vivo* context and form gel phases that need to be controlled by high volumes of cholesterol[2,98]. The release profile of Doxil also may be unfavorable for the *in vivo* applications, as there is evidence to suggest the lipid vesicles are not endocytosed by tumor cells but instead merely accumulate at the tumor site[2,98]. If this is truly the case, a faster release profile would be favorable so that doxorubicin concentrations in the tumor can reach cytotoxic concentrations prior to clearance. By including a gel core, liposome formulations like Doxil would ideally gain both stability and an added robust layer of lipid formulations that can synergistically target the tumor environment.

3.1.2.1 Influence of Fatty Acid Chain Disorder

An interesting and accidental finding of this study was the influence of fatty acid acyl chain disorder on the size of the LNG particles as demonstrated by the differences in DOPC and POPC. A summary of each PC molecules' relevant properties can be found in Table 3-3.

Table 3-3. Summary of PC lipid properties. Data courtesy Lipid Maps Structural Database, Avanti Polar Lipids, and Polyansky et al.[99].

LIPID	MELTING TEMPERATURE (T_M)	MISCIBILITY WITH DSPE (QUALITATIVE)	SPONTANEOUS CURVATURE (1/NM)	S_{CD} VECTOR
DOPC	-22 ˚C	Medium	-1/20	0.104
POPC	-3 ˚C	Low	~1	0.183/0.149

The primary reason for the different properties of these two molecules comes from the length and saturation of the lipid chains. DOPC contains two chains each 18 carbons long and with a double-bond at the 9th carbon. POPC contains one similar oleyl chain but also has a saturated 16 carbon palmitoyl chain. The result of POPC's shorter saturated chain is a near neutral ratio between its head group and tail group area, as illustrated by its lower spontaneous curvature, and an overall greater order in each chains S_{CD} vector.

As shown in Figure 3-1 and Figure 3-2, DOPC vesicles, in general, are larger with more polydispersity than POPC vesicles at low PEGDA concentration (POPC 118±5.98 nm versus DOPC 139±3.07 nm). However, at higher polymer concentrations, the vesicle size relationship to PC identity is reversed (POPC 298±31.6 nm versus DOPC 207 ± 8.43 nm). We hypothesize that the difference in size can again be attributed to molecular crowding (i.e. molecular hindrance to diffusive transport) and membrane packing (i.e. thermodynamics and stability of lipid self-assembly). At low polymer concentrations, in this instance 10% vol., the difference between POPC and DOPC LNG particles is statistically insignificant suggesting that the polymer is exerting little influence over liposome size. However, the difference between 50% vol. POPC and DOPC LNG particles is statistically significant ($P < 0.05$). There is likely significant molecular crowding at a 50% vol. concentration of PEGDA which would increase lipid diffusion time compared to a non-polymer solution. During the hydration, sonication, and extrusion steps the

liposome breaks causing lipid molecules to become initially dispersed in solution. The lipid molecules must then diffuse through the solution towards each other to form the lipid membrane. DOPC molecules prefer larger liposome diameters due to difficult membrane packing caused by the negative spontaneous curvature between their head and tail groups. DOPC should also be excluded faster from water than POPC due to their increased disorder which would disrupt solvation. We therefore hypothesize that the differences between DOPC and POPC liposome formation in the various PEGDA environments can be attributed to differences in the thermodynamics and the transport kinetics of self-assembly. Further experiments would need to confirm if these results are not linked to other parameters such as lipid concentration. It should be noted that these properties currently only reflect differences in surface tension between 3 mM DOPC and POPC bilayers with 15% mol cholesterol. Cholesterol is particularly important to consider given the proposed hypothesis as it is known to condense and order membrane packing thus reducing differences in the work of liposome formation.

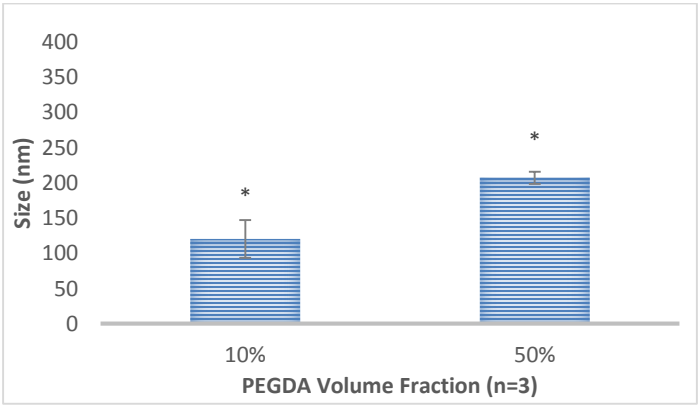

Figure 3-1. DOPC:Chol (85:15) vesicle size by PEGDA volume percentage. Error bars represent standard deviation and asterisks denote significant difference ($P < 0.05$).

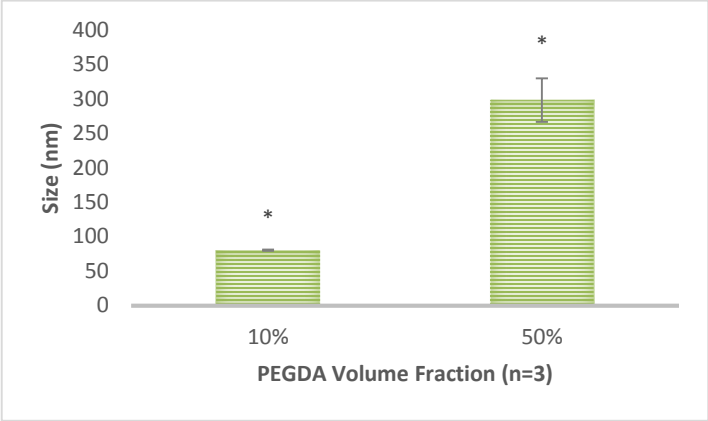

Figure 3-2. POPC:Chol (85:15) vesicle size by PEGDA volume percentage. Error bars represent standard deviation and asterisks denote significant difference ($P < 0.05$).

3.1.2.2 Influence of DSPE-PEG

In order to explore the influence of PEGylation on the fabrication protocol, PEG chains were added to the exterior of the LNGs by inclusion of PEG-conjugated DSPE lipids in the lipid film at 5% molar concentration. At this concentration, PEG chains should be in the brush regime on the exterior and interior of the lipid membrane[100]. We chose to include conjugated PEG chains for two primary reasons: First, exterior PEG chains provide a hydrophilic PEG corona that can inhibit protein adsorption and subsequently immune recognition; Second, to compare the influence of a PEG corona on the LNG particle stability with low transition temperature lipids to the standard Doxil formulation. The second purpose highlights a primary advantage that we hypothesized for liposome nanogel systems – an ability to use high fluidity lipid membranes without concern over drug leakage and loss in particle stability.

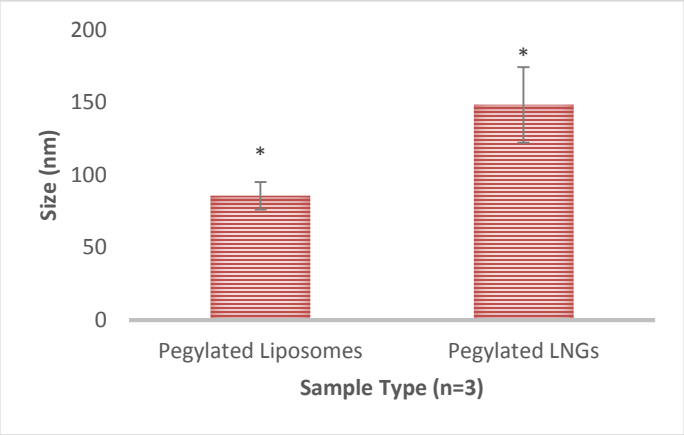

Figure 3-3. DOPC:Chol:DSPE-PEG(2000) (80:15:5) vesicle size for liposomes and LNG particles (PEGDA 10% v/v). Error bars represent standard deviation and asterisks denote significant difference ($P < 0.05$).

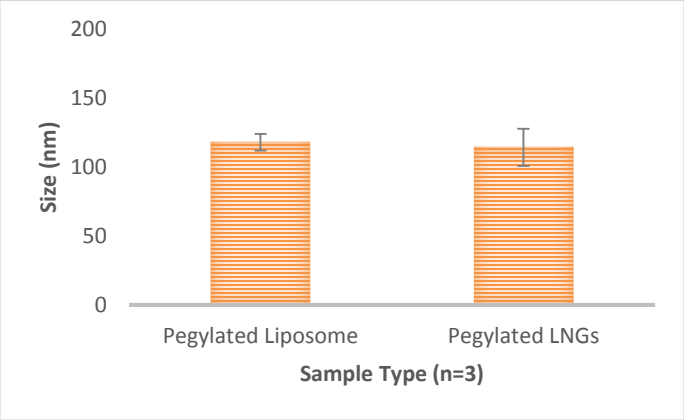

Figure 3-4. POPC:Chol:DSPE-PEG(2000) (80:15:5) vesicle size for liposomes and LNG particles (PEGDA 10% v/v). Error bars represent standard deviation.

Adding PEG to the lipid membrane had an influence on LNG size that varied according to the PC lipid membrane component. DOPC liposomes were highly influenced by the presence of PEG chains while POPC liposomes were only mildly influenced (Figure 3-3 and Figure 3-4). These results were surprising however we believe that the primary reason for this phenomenon is related to the miscibility of DSPE-PEG rather than caused by the PEG chains themselves. DOPC

is reported to have a poorer miscibility with 18 carbon fatty acid chain lipids, like DSPE, compared to POPC. A possible explanation is that the DSPE elements are exhibiting slight phase separation from the PC portion of the membrane causing the PEG chains to expand. The long chains then may interact with the polycarbonate filter during extrusion causing a smaller size distribution to be stable during the repetitive breaking and reformation process.

3.1.3 Varying the Extent of Sonication and Extrusion

After forming an MLV solution, two steps were taken in an attempt to size the liposomes into 100 nm SUVs: Sonication and Extrusion.

3.1.3.1 Pros and Cons of Sonication

Sonication is a technique in which the liposome solution is subjected to high frequency vibrations. These vibrations resonate with specific sizes of liposomes causing them to expand and collapse upon retraction. Therefore, if subjected for an appropriate duration of time, sonication is a good technique for forcing the intrinsically unstable large vesicles to break and reform as smaller vesicles. Sonication can be performed in one of two ways: tip sonication or bath sonication. Tip sonication applies the high frequency vibrations to the lipid solution through the use of an ultrasonic probe placed directly in the solution while bath sonication transfers vibrations through an aqueous bath to the solution container. We choose to use tip sonication as it is capable of a direct transfer of energy allowing for greater vibrational translation into the solution. Bath sonication was also tested however it proved to be too weak for the high viscosity of the pre-polymer solution.

Tip sonication proved to be effective at primarily disrupting the multiple lamella of the larger vesicles. We observed this trend after preparation of two 50% volume PEGDA LNG samples with either 8 intervals of 1 minute exposure to the sonication tip or 4 intervals of 2 minutes of exposure to the titanium tip. During exposure both samples were kept in an ice bath to minimize heat damage. The increased time of exposure per round led to a greater absorption of energy, which was confirmed by the degree of melting of each ice bath. When evaluated using DLS, both samples had similar size, but Cryo-TEM revealed that the sample that had received less sonication contained large multilamellar vesicles (Figure 3-5). These vesicles may have appeared due to the Cryo-TEM preparation process, however, we did not have a problem with any other sample prepared using the same parameters. This trend did not exist for 10% volume PEGDA samples suggesting that the use of sonication is only necessary for 50% volume PEGDA LNG samples. All samples prepared with doxorubicin content were not prepared with sonication in hopes of preserving the integrity of the lipid membranes.

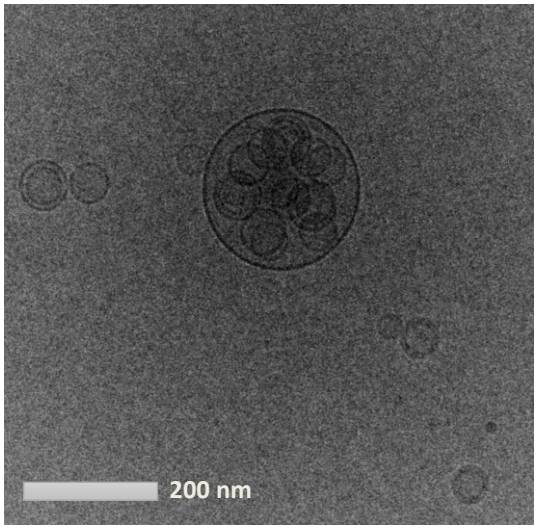

Figure 3-5. Cryo-TEM image of large DOPC:Chol:DSPE-PEG(2000) (80:15:5) multilamellar LNG vesicles (PEGDA 50%) prepared by 4 intervals of 1 minute exposure to tip sonication and 11 passes through a 100 nm membrane and an 80 nm membrane.

3.1.3.2 Multiple Extrusion Protocols

Extrusion is a simple procedure to size liposomes by passing the solution through nanoporous polycarbonate filters. Similar to sonication, larger vesicles are broken during the contraction the vesicles are forced to undergo to pass through the filter. Over many passes, the breaking and reforming of larger vesicles enriches a small, stable dispersion of liposomes with an average diameter close to that of the membrane pore size (±10-20%[46]). We employed two simple methods to fabricate 100 nm LNGs: One in which we extruded the liposome solution through a 100 nm filter 11 times followed by extrusion through an 80 nm filter 11 more times and another protocol in which we passed the liposome solution through a 100 nm and 80 nm stacked filter set for a total of 11 passes. As shown in Table 3-4, these protocols showed no significant difference when considering the size of LNGs after encapsulation of doxorubicin. However, it became clear during PC assay tests to measure the lipid concentration that extrusion decreased the overall lipid content by 1/3. Therefore, we choose to use the second protocol as it was simpler and reduced the chance to lose liposome solution.

Table 3-4. Summary of size and uniformity of POPC:Chol:DSPE-PEG(2000) (80:15:5) LNG patirlces (15% wt/wt) prepared using each extrusion technique. Standard deviation is from 3 samples explicitly made for this experiment.

	AVERAGE (NM)	**PDI**	**STD AVG (NM)**	**STD PDI**
STEP-WISE EXTRUSION	123	0.101	11.9	0.046
STACKED MEMBRANE EXTRUSION	127	0.099	5.89	0.030

3.1.4 Bulk Phase Photoinitiator Removal Protocols

Three distinct methods were employed to remove bulk phase photoinitiator: dialysis, dilution, and column buffer exchange. We evaluated each by assessing their ability to prevent bulk phase polymerization and the influence each had upon vesicle stability and size. Between dialysis and dilution, dialysis appears to produce slightly better results for preparation of POPC LNG particles (e.g. smaller size, less polydisperse) however the results are insignificant (Table 3-5).

Table 3-5. Summary of bulk phase removal data for preparation of POPC:Chol:DSPE-PEG(2000) (80:15:5) LNG particles (15% wt/wt) prepared by extrusion through a 100 nm and 80 nm nanoporous filter.

	AVERAGE (NM)	**PDI**	**STD. AVG. (NM)**	**STD. PDI**
DIALYSIS(MWCO 3500)	80.2	0.150	1.05	0.039
DILUTION (5X VOLUME)	85.6	0.172	9.48	0.031
BUFFER EXCHANGE (0.15 M NACL)	106	0.160	5.58	0.089

The primary difference between the two protocols is the final volume and consequently the final LNG concentration. In order to avoid secondary processing, dialysis was preferred over dilution as a way to reduce the final solution volume while also providing an easy means to remove non-encapsulated agents during the fabrication process. Similarly, column chromatography buffer exchange was preferred over dialysis not on the basis of nanoparticle properties but on flexibility with drug loading protocol. Both protocols similarly removed bulk phase photoinitiator and prepared uniform samples, however, column buffer exchange proved to be faster in execution allowing for greater data acquisition. Overall, we believe column chromatography buffer exchange to be a simple way to remove excess photoinitiator as well as establish ionic gradients and remove non-encapsulated molecules from solution.

3.1.5 Particle Morphology and the Hydrogel Core

In order to evaluate particle morphology, we used scanning electron microscopy (SEM), to view the nanoparticles in a non-hydrated state, and cryogenic transmission electron microscopy (Cryo-TEM) to view the particles incased in vitreous ice.

3.1.5.1 SEM

In preparation for SEM, we allowed LNG samples to dry on a clean glass coverslip and then sputter coated the samples with Iridium to improve conductivity. We used this procedure as a method to view the nanogel core as the liposome exterior should dry and aggregate in this process. As shown in Figure 3-6, we believe these large, folded structures that appeared at the center of the dried drop to be the lipid aggregates. Nanoparticles however could be found within the folded lipid matrix as well as on the exterior of the dried drop, which is where images like those in Figure 3-7 were taken. We noticed that the nanoparticle morphology was often either ellipsoidal or spherical. We hypothesized that the ellipsoidal morphologies resulted from spherical particles that flattened out on the glass cover slip during the drying process. This explanation was further suggested by the agreement between DLS readings and the spherical LNG particles but not with the ellipsoidal radii particles seen in the SEM images. We also however acknowledged another possible explanation that the liposome population is heterogeneously split between spherical and ellipsoidal liposomes. Therefore we chose to turn to Cryo-TEM to observe the particles in a hydrated state.

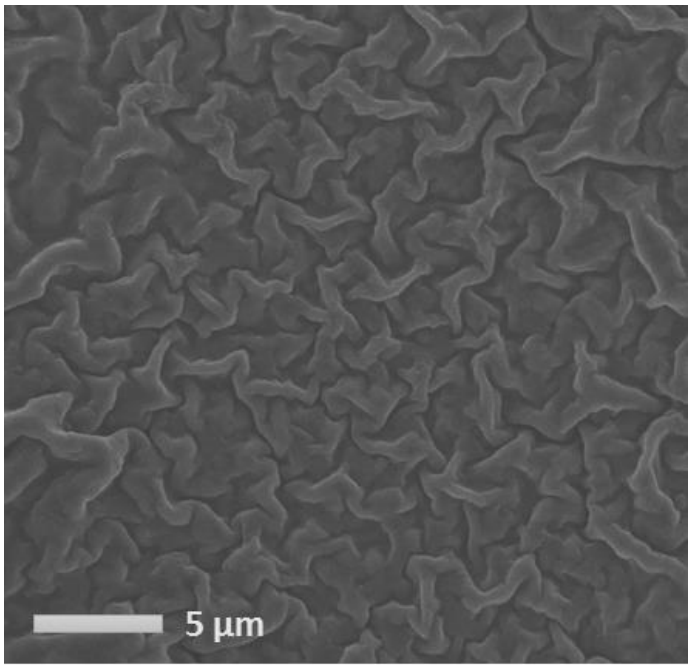

Figure 3-6. SEM image of an area in the center of a dried POPC:Chol (85:15) LNG particle (50% v/v PEGDA) sample on a microscope coverslip and sputter coated with Iridium.

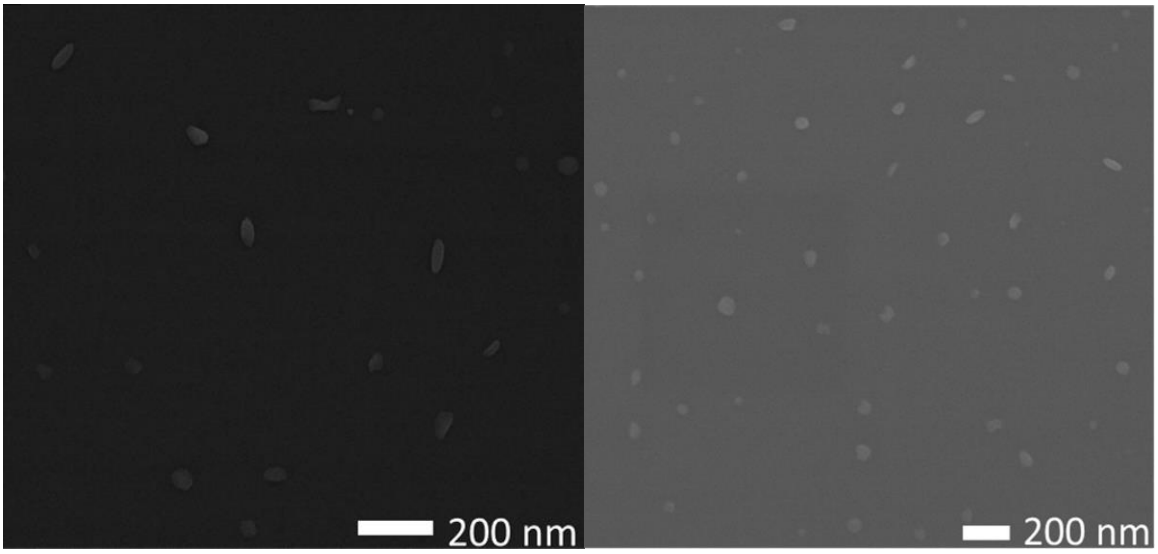

Figure 3-7. SEM image of an area near the outer edge of a dried POPC:Chol (85:15) LNG particle (50% v/v PEGDA) sample on a microscope coverslip and sputter coated with Iridium.

3.1.5.2 Cryo-TEM

LNG samples were prepared for Cryo-TEM by flash freezing a drop of the solution in liquid ethane that had been suspended on a copper grid. The primary benefit of imaging samples with this technique is that the liposome exterior of the LNG particles is preserved in its hydrated state. We pursued a cryogenic analysis of particle morphology for two primary reasons: First, we hoped to be able to visualize the hydrogel core inside of the liposomes; second, we wanted to confirm our hypothesis that the ellipsoidal particles seen in SEM occurred due to the flattening out of spherical vesicles. As shown in Figure 3-8, all LNG particles imaged were spherical in nature. However, we also noticed that the particles in general were smaller than expected. The sample in Figure 3-8 corresponds to the DLS data shown in Figure 3-9.

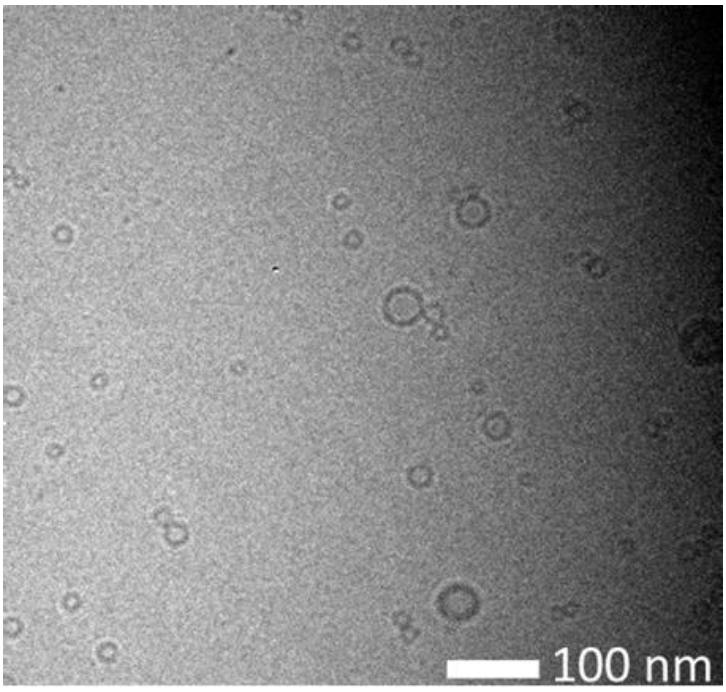

Figure 3-8. Cryo-TEM image of DOPC:Chol:DSPE-PEG(2000) LNG particles (15% wt/wt) prepared with 4 intervals of 2 minutes exposure to a tip sonicator and extrusion through a 100 nm and 80 nm nanoporous filter.

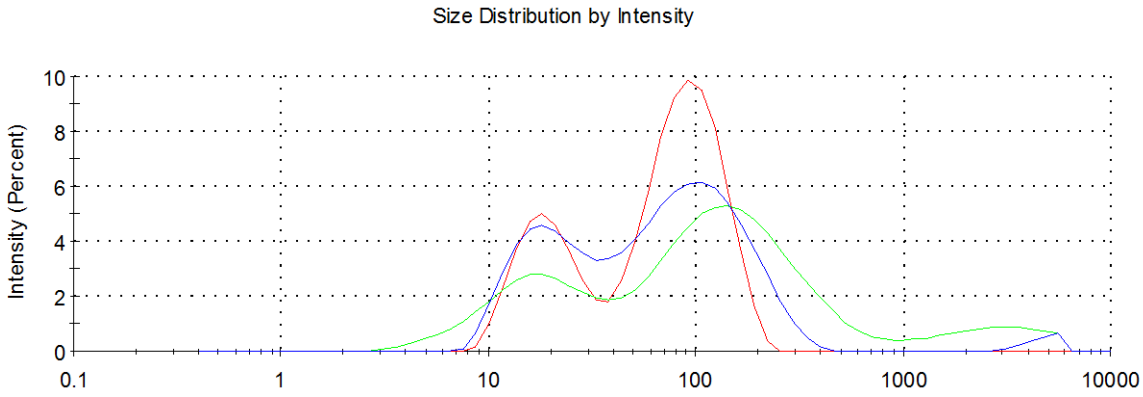

Figure 3-9. DLS size distribution of the three DOPC:Chol:DSPE-PEG(2000) LNG samples imaged. The red peak corresponds to Figure 3-8.

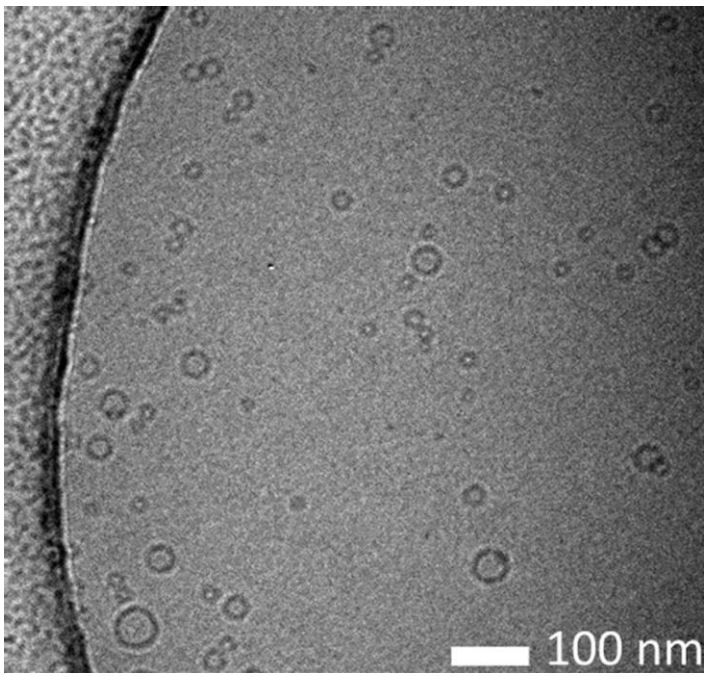

Figure 3-10. Cryo-TEM image of DOPC:Chol:DSPE-PEG(2000) LNG particles near the edge of the cooper grid.

As shown in the DLS data in Figure 3-9, a population with a peak of ~20nm is expected and is visible in the Cryo-TEM image. However, the ~80nm population was less prominent in the image and many of the vesicles imaged were naturally smaller. Therefore, we believe that this

may be a result of the procedure used to the flash-freeze the LNG solution. Depending on the blotting settings during sample prepartion, LNG particles of a particular size may have been excluded. As shown in Figure 3-10, the majority of the LNG particles that were observed in Cryo-TEM were found near the edges of the viewing wells in the copper grid. Further studies will be necessary to confirm our hypothesis regarding the spherical particles. It was also clear that a separate method would be necessary to prove the hydrogel core was indeed what was being visualized in the SEM images as there was not a significant contrast between the liposome core and the exterior vitreous ice.

3.1.5.3 Destabilizing the Liposome Membrane

As was mentioned in the previous section, the nanogel core of the LNG particles was not sufficiently evident in the Cryo-TEM images as we had hoped. Therefore we chose to use a simple method that had been used previously to disrupt the liposome exterior[101]. In this assay, a sample is prepared and then measured using DLS to obtain a baseline reading. A detergent is then added to the solution to disrupt the liposomal membrane. We chose to use 15% volume TX-100 as it was readily available and it had been previously used in literature for the same purpose[101]. A non-polymerized sample was also subjected to this assay to ensure to evaluate if the presence of polymer alone, without radical polymerization to develop an entangled lattice, was sufficient to resist the detergent. As shown in Figure 3-11, the peak at ~120 nm was disrupted in the second DLS reading of the polymerized LNG solution and two smaller peaks were generated (Note the particles are larger than normal as Doxorubicn was encapsulated during this test). These peaks were also present in the second reading of the non-polymerized sample while the primary peak was absent. Combined, this assay confirms that UV radiation polymerizes a nanogel core within the liposomal lumen that can resist detergent breakdown.

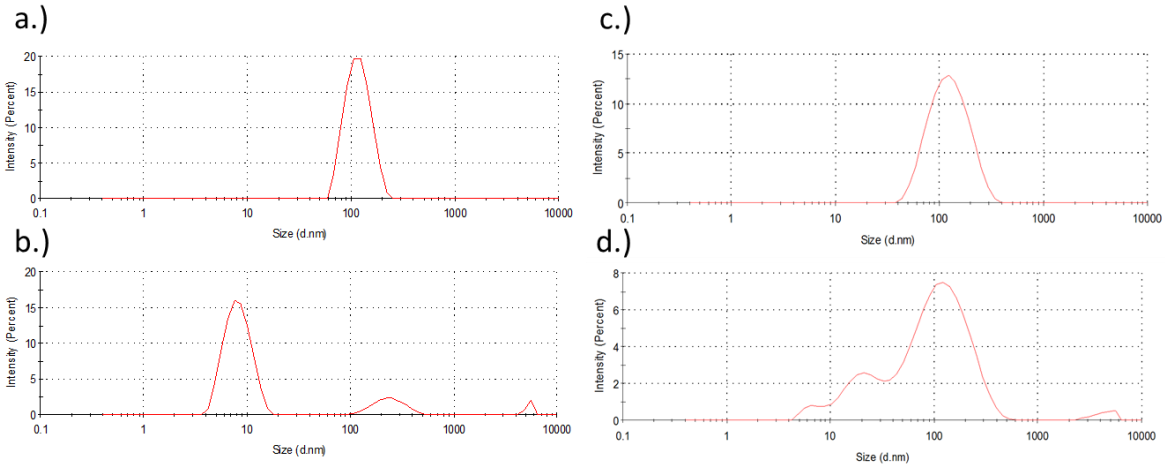

Figure 3-11. DLS measurements of liposomes (a-b) and POPC:Chol:DSPE-PEG(2000) LNG particles (15% wt/wt) (c-d) in 15% TX-100. a.) DLS measurement of non-polymerized liposome prior to addition of detergent. b.) Liposome size measurement after addition of 15% TX-100 c.) DLS measurement of LNG particles prior to addition of detergent. d.) LNG particle size measurement after addition of 15% TX-100.

3.1.6 Stability and Surface Charge

We analyzed the colloidal stability of LNG particles in aqueous media by monitoring the size of the particles in room temperature solution every 24 hours for a week. There was no significant increase in the size in the particles over this time confirming the LNG solution is colloidal and stable. We also attempted to perform zeta potential measurements to gain a sense of the surface charge present on the LNG surface. Only one reading however was gathered as all previous days did not provide a significant signal for the Malvern zetasizer to produce a confident measurement. The low signal generated by the particles was a consistent problem for all LNG solutions produced and it is unclear why we were unable to read the surface potential in general. Enough measurements were made to be able to assert that the nanoparticles however are in general significantly negative when Rho-PE is included in the lipid membrane. We also prepared POPC LNG samples with 5% mol POPS in an attempt to produce a strongly negative surface

charge, however, no significant difference was observed between POPC:Chol (85:15) LNG particles and POPC:Chol:POPS (80:15:5) particles (Figure 3-12). Future studies will be needed to analyze the charge composition of these particles.

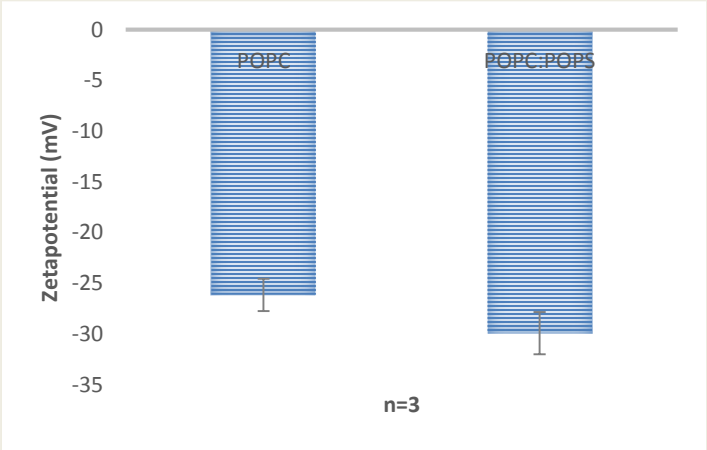

Figure 3-12. Zetapotential of POPC:Chol (85:15) LNG particles (PEGDA 50% v/v) and POPC:Chol:POPS (80:15:5) LNG particles (PEGDA 50% v/v). Error bars represent standard deviation.

We also analyzed the serum stability of the LNG particles in 50% FBS at room temperature for 5 days. As shown in Figure 3-13, the LNG particles remained stable for 3 days prior to formation of large aggregates. Unperturbed particles did persist in solution, however, the PDI of the solution rose to be above 0.5 for the remainder of the assay. These results are a setback compared to the Doxil formulation that is stable in serum for several weeks[2]. The LNG lipid composition does have the same amount of PEGylation, however, it has significantly less cholesterol (20% versus 45% for Doxil). Cholesterol may play an important role in preventing proteins from penetrating the lipid membrane and creating stable protein monolayers[46].

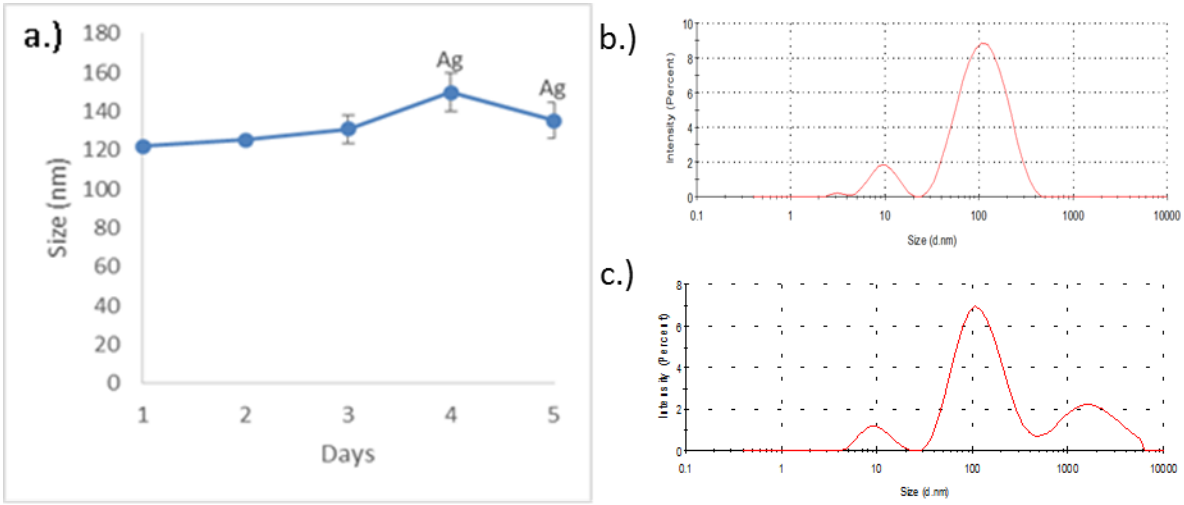

Figure 3-13.) Serum stability of LNG particles in 50% FBS. a.) Average size measurements of POPC:Chol:DSPE-PEG(2000) LNG particles (15% wt/wt) in 50% FBS solution monitored over 5 days. Error bars represent standard deviation and "Ag" denotes the formation of large protein aggregates in solution. b.) DLS measurement from day 1 c.) DLS measurement from day 5

3.2 Encapsulation of Doxorubicin and Rhodamine123

The primary aim of this project was the development of a highly customizable nanoparticle fabrication system that can be used for the delivery of a variety of therapeutic agents to cells. Due to the nature of the fabrication system, hydrophilic small molecules are prime targets for this form of nanoparticle. We evaluated "passive" encapsulation of a model hydrophilic compound rhodamine123 during the hydration of the lipid film. We also demonstrated that the ammonium sulfate gradient, a high efficiency ionic gradient method for loading weak amphipathic bases[2,47,92,98], was compatible with this system.

3.2.1 Passive Encapsulation during Hydration of the Lipid Film

Encapsulation of molecules during hydration or rehydration of lipid films during liposome preparation is considered passive here because there are no active gradients present in

the system outside of diffusion. Previous studies have shown that the upper limit of the encapsulation efficiency for this method is ~80%[102]. However, to achieve ~80% encapsulation efficiency, it is necessary to use freeze-thaw cycles as well as freeze drying and rehydration. All these steps drastically increase the complexity of fabrication for a LNG system therefore we choose to evaluate how easily hydrophilic components could be encapsulated during the hydration of the lipid film without any further modification of our liposome preparation protocol.

Rhodamine123 is a hydrophilic small molecule with excitation and emission peaks at 480 nm and 530 nm respectively. To assess the stability and encapsulation of rhodamine123 throughout the fabrication process, a calibration curve was made using known concentrations in deionized water. We found that the fabrication process is responsible for the loss of 32±2.4% prior to any attempt to remove non-encapsulated agent. There are two primary contributions to this loss in fluorescent intensity outside of photobleaching. The most obvious is the loss of solution volume during fabrication. The samples used to generate this data were all subjected to sonication and extrusion. According to our data, sonication is usually responsible for losses of volume on the order of 10s of µL, however extrusion can result in volume losses of 100 µL. As was noted previously, PC assays revealed that approximately 1/3 of all lipid components were lost during the extrusion process when compared to the theoretical maximum. The second reason may be that the fluorescence also decreases due to liposomal filtering of the fluorescent signal. It is a known phenomenon that the lipid bilayer of the liposome partially shields fluorescent molecules from excitation and also absorbs some of the fluorescent emission spectra[94]. Depending on context this effect can be particularly devastating towards accurate results. It is difficult to assess from the data the contribution of both effects however it is my personal opinion that volume losses to extrusion and sonication are the likely culprits. Evaluation of each effect could be determined using an agent with a known absorbance spectra like doxorubicin, however we felt that this assay would unnecessarily contaminate equipment with a cytotoxic element and

would be a waste of valuable anthracycline. Therefore, we chose to employ two separate encapsulation measurements to account for the fluorescent quenching. In the following experiments, encapsulation efficiency was determined by equation 3-1 and a "procedural" loading efficiency was determined by equation 3-2.

Eq. 3-1 $$Encapsulation\ Efficency = \frac{Amount\ Measured}{Amount\ Initially\ Added} * 100$$

Eq. 3-2 $$Procedural\ Loading\ Efficiency = \frac{Amount\ Measured}{Amount\ Prior\ to\ Bulk\ Phase\ Removal} * 100$$

In terms of the equations, encapsulation efficiency is a measure of the overall efficiency of the system with regards to the initial concentration of rhodamine123. Procedural loading efficiency is the measure of the how much of the signal measured, prior to removal of the bulk phase, originated from the encapsulated agent. Taken together, these two measurements provide a sense for how much of the signal is truly filtered out.

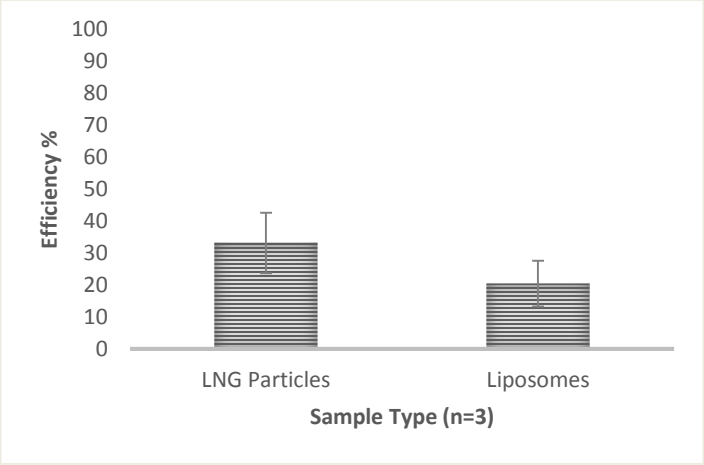

Figure 3-14. Encapsulation efficiency of rhodamine123 in POPC:Chol:DSPE-PEG(2000) (80:15:5) LNG particles (15% wt/wt) and liposomes. Error bars represent standard deviation.

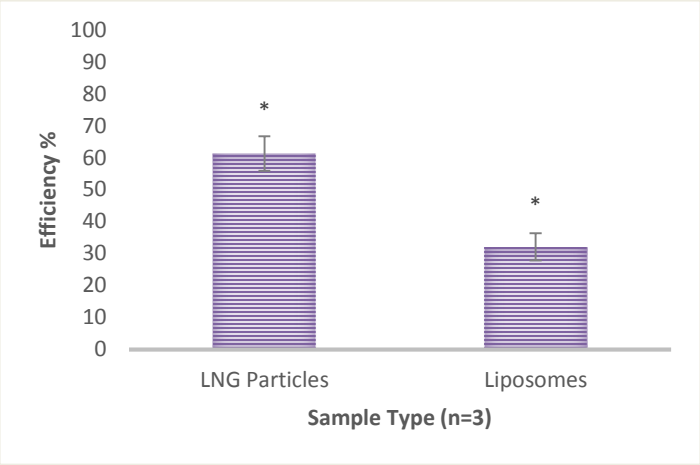

Figure 3-15. Procedural loading efficiency of rhodamine123 in POPC:Chol:DSPE-PEG(2000) (80:15:5) LNG particles (15% wt/wt) and liposomes. Error bars represent standard deviation and asterisks denote significant difference ($P < 0.05$).

Figures 3-14 and 3-15 present the measurement of both encapsulation efficiency and procedural loading efficiency for a 10% vol PEGDA LNG solution versus a control nanoliposome without a PEGDA gel core. Bulk phase rhodamine123 and photoinitiator were both removed using dialysis for this particular sample. In both instances, the average encapsulation and procedural loading efficiencies are higher for the gel-filled particles however the difference is only significant for the drug loading efficiency. Qualitatively, the difference between the liposome and polymerized LNG encapsulation and procedural loading efficiencies can be attributed to differences in retention and fluorescent quenching combined. The polymerization of the LNG core and the presence of PEGDA in solution appear to help retain rhodamine123 by about 13% overall, or 29% with respect to the signal prior the removal of the free dye. These results are especially interesting considering that polymerization does not take place until removal of the bulk photoinitiator using dialysis. One potential explanation is that the viscous influence of PEGDA in solution during sonication and extrusion helps to lessen rhodamine123 escape from the interior of the liposome. Molecular crowding, in this instance, may act to prevent the dye from being sent into the bulk phase where it is removed during dialysis.

3.2.2 Ammonium Sulfate Gradient Encapsulation of Doxorubicin

The ammonium sulfate gradient is a model ionic gradient that was first developed for use in the preparation of the liposomal doxorubicin blend, also known as Doxil[2,47,92]. In this method, ionic agents are segregated between the lumen of the liposome and the bulk using a buffer exchange creating a strong gradient. To achieve this gradient, the ionic components of the salt must have significantly different octanodiol partition coefficients (i.e. ability to cross the lipid membrane) and affinities for the drug of interest. Ammonium sulfate is excellent for this reason as ammonium ions easily exit the liposome and sulfate ions form complexes with weak amphipathic bases. Doxorubicin in particular complexes with sulfate ions and self-aggregates to form a condensed crystal phase visible in Cryo-TEM[2,47,92]. During this transition, the absorbance of doxorubicin shifts from 470 nm to 550 nm due to changes in pH that occur during aggregation, thus providing a simple measurement of the degree of crystallization[92]. It is important that the buffer used to remove the ammonium sulfate from the bulk phase would only have weak interaction with the drug being loaded as well as biological compatibility. We analyzed sodium citrate and sodium chloride due to previous use in this procedure[2,17,92,96].

3.2.2.1 Buffer Exchange with Sodium Citrate

Sodium citrate has been documented in the past for buffer exchange in the establishment of the ammonium sulfate gradient[17]. Using a Sephandex G-25M column, we created a strong gradient between the bulk phase and the lumen of the liposome. We then measured the PC lipid content of the solution using a PC hydrolysis assay and added 0.2 mg doxorubicin for every mg of PC. The solution was then allowed to stir overnight (~10 hours) before being passed through another column to remove non-encapsulated Doxorubicin. Afterwards the solution was exposed

to UV for 5 minutes to polymerize the LNG solution prior to reading the absorbance at 470 nm, 492 nm, and 550 nm. From the absorbance data, an encapsulation efficiency was calculated using equation 3-1. The degree of doxorubicin aggregation was quantified by the ratio between the absorbance at 470 nm and 550 nm as mentioned previously. The results for sodium citrate, summarized in Table 3-6 alongside the results for sodium chloride, were particularly underwhelming compared to the account given in literature. One possible explanation for this could arise from the presence of PEGDA and the photointiator in solution. Citrate is known to bind and stabilize doxorubicin aggregation given the right solution conditions[92]. Although we attempted to increase the acidity to a pH of 5, PEGDA and the photoinitiator may have absorbed free protons increasing the basic nature of the solution to a point where citrate would favorably bind doxorubicin. Large doxorubicin fibers were noticeable in solution and precipitated out of solution when the solution was subjected to 20,000 g for 30 minutes. We investigated the kinetics of encapsulation with sodium citrate and found only a slight increase in doxorubicin fluorescent bleaching when incubated with liposomes with a prepared gradient in pre-polymer solution versus an aqueous doxorubicin mixture. Although this experiment did not include a polymer-free liposome control, the data suggests that PEGDA and the photointiator disrupt the ammonium sulfate gradient when combined with sodium citrate assuming negligible differences from the previous preparation. A proper control, however, may reveal that the lipid membrane composition was not suitable for the proper segregation of the ions.

Table 3-6. Encapsulation and aggregation of doxorubicin in LNG particles. Error corresponds to standard deviation.

	ENCAPSULATION EFFICIENCY	470/550 ABSORBANCE RATIO
0.155 M SODIUM CITRATE	17±1.9%	2.57±1.2
0.15 M SODIUM CHLORIDE	97±2.7%	1.65±0.02

3.2.2.2 Buffer Exchange with Sodium Chloride

Since sodium citrate appeared incompatible with the hydrogel system used in this study, we chose to employ sodium chloride due to its simplicity. We hypothesized the primary advantage was that the chloride ion was less likely to have a strong interactions with any of the elements within the solution. Additionally, sodium chloride was used for this approach in the original patent for the ammonium sulfate gradient[2]. Following the same protocol used for sodium citrate with adapted concentrations for sodium chloride, we found that sodium chloride was extremely effective at setting up a stable ammonium sulfate gradient, resulting in encapsulation efficiencies of 97±2.7%. It is important to note that the encapsulation efficiency was calculated in the same way it had been for rhodamine123 (Eq 3-1), where the maximum amount added was 0.2 mg doxorubicin per mg PC. Small errors may have resulted due to natural error in the PC hydrolysis assay. However, given enough time the encapsulation efficiency was always near 100%. To prove time was an important parameter we performed two experiments. First, we incubated the non-polymerized LNG solution with doxorubicin for 3, 6, 9 hours to determine how important time was in the incubation. The data from this experiment is Figure 3-16.

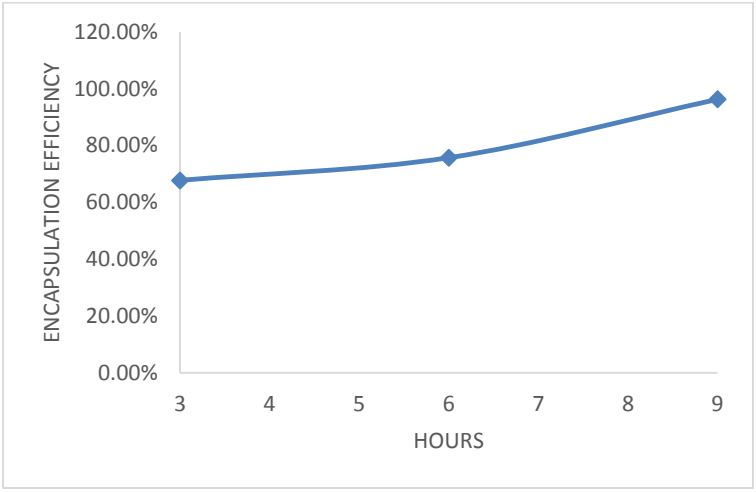

Figure 3-16. Encapsulation efficiency of doxorubicin versus incubation time for POPC:Chol:DSPE-PEG(2000) (80:15:5) LNG particles (15% wt/wt) pre-polymerization.

It was fairly obvious from this simple experiment that a correlation between time and encapsulation efficiency existed as we expected. Second, similar to experiments done with sodium citrate, we analyzed the fluorescent quenching that takes place as doxorubicin aggregates with sulfate inside the liposome. Ideally, the final fluorescence of the sulfate doxorubicin complex would be completely quenched. We analyzed the system using a multiplate reader and determined a loading constant of 0.34±0.024% per minute, or approximately 6.6 pM/min, assuming a first order kinetic equation. The graph of this data is shown in Figure 3-17. Although this loading constant is very slow, given enough time, as was demonstrated earlier, the end result is a high degree of stable encapsulation.

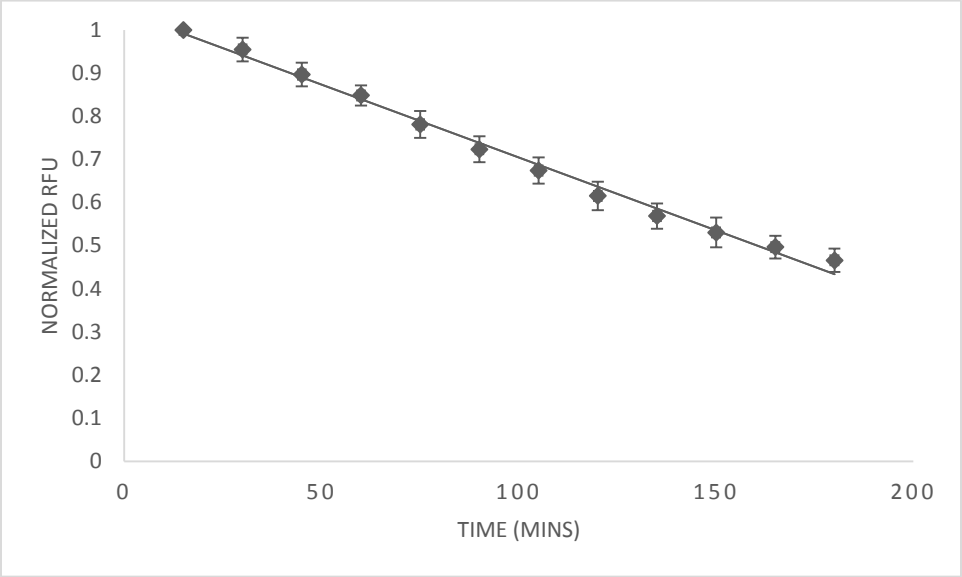

Figure 3-17. Encapsulation of doxorubicin versus time using sodium chloride 0.15 M for POPC:Chol:DSPE-PEG(2000) (80:15:5) LNG particles (15% wt/wt) pre-polymerization. A well of an equal concentration of aqueous doxorubicin was used to correct for photobleaching. Values were normalized by the initial RFU reading. Error bars represent standard deviation.

3.2.3 Release of Doxorubicin from Polymerized Vesicles

The release profile of a drug from a nanoparticle system is crucial in determining the primary benefit of encapsulating the agent. We sought to evaluate the release of doxorubicin from polymerized LNG particles to determine if the hydrogel matrix is effective at hindering doxorubicin crystals from disassociating and precipitating out of the liposomes. To this end, we fabricated three samples of 3 mL of LNG particles each with encapsulated doxorubicin at a ratio of 0.2 mg doxorubicin/mg PC and placed the samples in 3500 MWCO dialysis bags for incubation in 3 L of 1X PBS. The absorbance of a 100 µL sample from each bag was measured at various time points to determine the amount of doxorubicin that had leaked from the bag as well as the state of the doxorubicin aggregation. The release profile and 470/550 nm aggregation ratio are presented in Figure 3-18 and Figure 3-19 for both polymerized and non-polymerized LNGs. We were surprised to find that the release from the LNG particles was bi-phasic. The first phase

is reminiscent of a typical osmotic burst that occurs from nanoparticles when subjected to a strong diffusion gradient. The second phase, however, corresponded with a sudden collapse of the doxorubicin aggregation followed by a subsequent recovery to a more condensed aggregation ratio (Figure 3-19). We were also surprised to observe that an non-polymerized core had a significantly delayed release compared to reports of release from liposomes of a similar blend[2,46]. Polymerization only had one point of significant difference from non-polymerized LNG at the 96 hour time point. The 470/550 ratio shows that the doxorubicin crystal is more stable in the non-polymerized LNG and disassociation is not responsible for release. This is in direct contrast to the polymerized LNG that has a second phase directly corresponding for an initial collapse and recovery of doxorubicin aggregation. This finding presents an interesting paradigm where the simple inclusion of hydrophilic polymer could drastically increase stability without polymerization.

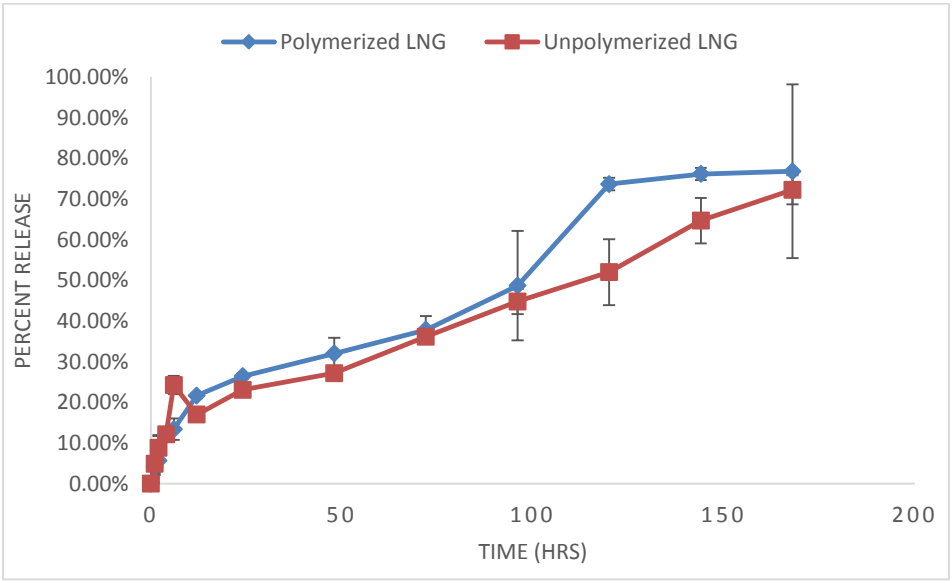

Figure 3-18. Doxorubicin release POPC:Chol:DSPE-PEG(2000) (80:15:5) LNG particles (15% wt/wt) post-polymerization in 3L 1x PBS. Error bars represent standard deviation.

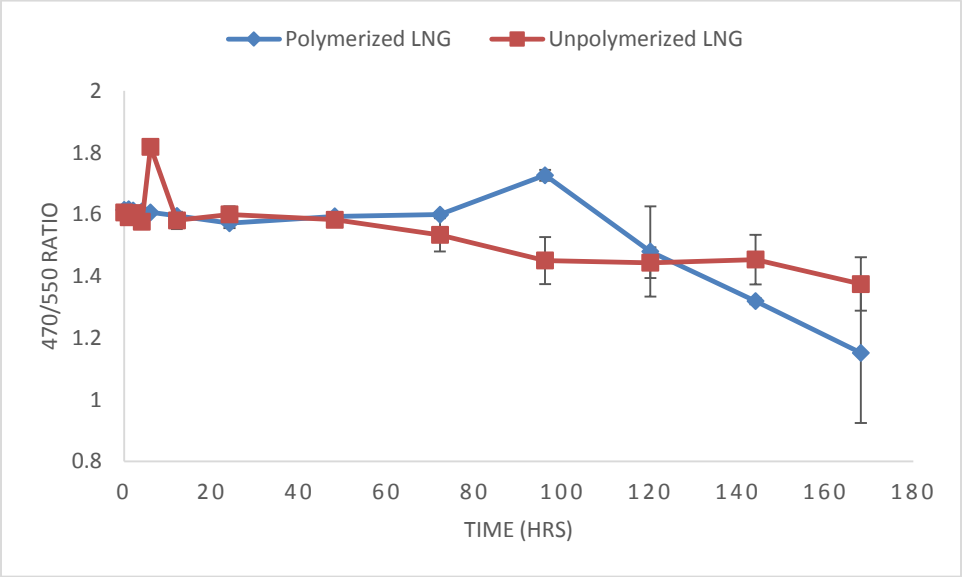

Figure 3-19. Doxorubicin crystal stability measured as a function of the 470/550 absorbance ratio during doxorubicin efflux from POPC:Chol:DSPE-PEG(2000) (80:15:5) LNG particles (15% wt/wt) post-polymerization. Data corresponds to Figure 3-17. Error bars represent standard deviation.

Overall, this finding is in agreement with our initial hypothesis that the inclusion of a hydrogel core would allow the use of a more diverse lipid component than is typically possible. We demonstrated delayed release this with a liposome exterior fabricated from a PC lipid component of a much lower Tg than the typical, long chain lipids used in typical Doxil/Caelyx fabrications[2,47]. The increased fluidity has been commonly blamed for doxorubicin leakage[2] resulting in release of ~50% of doxorubicin content in 1 hr[46]. However inclusion of the hydrogel matrix delayed release of 50% of the doxorubicin content past 100 hrs in both polymerized and non-polymerized samples. Therefore, we believe that the hydrogel core, or simply PEGDA polymer in solution, drastically increases the stability of the doxorubicin crystals within the liposome, as evidenced by little change in the 470/550 absorbance ratio, which may relate to improved release at the tumor site if appropriately targeted. We also find it worth further investigation regarding why a non-polymerized core stabilized the doxorubicin crystal better than the polymerized LNG. It may be that polymerizing the hydrogel prevents re-aggregation of

disassociated doxorubicin molecules by restricting molecular movement. Prolonged release studies past one week may reveal, however, that a polymerized core produces a core that is significantly more stable despite the burst release on the fourth day.

Chapter 4

Future Research and Considerations

Due to unfortunate circumstances, some of the aspects of this thesis could not be fleshed out as much as we would have hoped. In particular, two main areas deserve further assessment: stability and release. The stability of the LNG particles has been evaluated in aqueous media over the period of week as well as in fetal bovine serum over the period of five days. Long term studies are needed to assess the stability of each system both on the shelf and in a biological environment. It also remains unclear whether changes in the LNG zeta potential occur overtime due to difficulty achieving measurements. I predict that the charge will not change substantially due to the PEG chains on the surface but it is necessary to confirm this hypothesis. A final aspect of stability that is crucial is the ability of the LNG particles to resist deformation and rupture during inject and in extremely turbulent flow. We demonstrated that the LNG particles resist complete breakdown in high percentage detergent however more evidence about physical rupture is necessary. This may be an interesting option for ultrasound-oriented delivery[83].

The release properties of the LNG particles are also difficult to evaluate over the course of a week. Our data suggests that the hydrogel core, polymerized or non-polymerized, helps to stabilize the doxorubicin crystal aggregate. We have based this upon absorbance readings coupled with efflux of doxorubicin out of dialysis bags. Unfortunately, the release we have evaluated from the LNG particle is simplistic and a poor representation of the *in vivo* environment. Our data provides a starting point for assessment but it is necessary to evaluate the LNG particles in a cellular context as well as in animal models. It is also unclear how significant the difference a hydrogel core provides on the release of doxorubicin from liposomes without polymer in the

intraliposomal space. While our data deviates from the rapid release seen in literature[46], it is necessary to use a liposome control in the future to evaluate the exact benefit. We did not do so as we predicted a strong difference between polymerized and non-polymerized LNG particles. It may be that the polymer addition to the liposome has other effects outside of stabilization of the doxorubicin crystal.

There also exists a great opportunity to demonstrate further control over the physicochemical properties of the LNG particle. One of the main reasons we were initially attracted to the idea of a LNG particle was the ability to control a two component system. As was mentioned in the introduction, both the lipid composition and the hydrogel material can be tuned to have select sensitivities to environmental and clinician-derived stimuli. This would be a powerful opportunity to demonstrate robust control over molecular efflux. It would also be desirable to demonstrate that control over the lipid composition of the system would result in control over size and shape. In terms of the lipid component, although we present that the fatty acid chain composition of the liposome had an influence on the vesicle size at 3 mM concentrations it remains unclear the exact mechanism at play. Although we offer a hypothesis, It is unclear the validity of our claim or if these correlations will stay true with non-PC head group lipids. This same sentiment holds true for changes in size with polymer concentration. Future studies will need to evaluate the theories put forth to carefully the mechanism behind the polymer hindrance of sub-200 nm nanoliposomes.

In conclusion, this thesis presents the fabrication of LNG particles with details regarding size, shape, stability, encapsulation efficiency, and release. LNG particles have been demonstrated to be monodisperse and approximately 100 nm in size. Polymerization of the hydrogel core was proved using detergents and electron microscopy. The lamellarity and size were also confirmed by cryo-TEM. We used rhodamine123 and doxorubicin to demonstrate the encapsulation of hydrophilic small molecules using both a passive encapsulation technique and an

active transmembrane gradient. The release of doxorubicin was then used to demonstrate the influence a hydrogel core on release from a liposome based nanoparticle system. We are pleased to show that the release and encapsulation of doxorubicin are favorable compared to previous literature. Future studies should look to expand upon the release and physicochemical characteristics of these particles in order to take full advantage of the two component design.

Bibliography

1. Min, Y.; Caster, J. M.; Eblan, M. J.; Wang, A. Z. Clinical Translation of Nanomedicine. *Chemical Reviews* **2015**, 150619062806005.

2. Barenholz, Y. (Chezy) Doxil® — The First FDA-Approved Nano-Drug: Lessons Learned. *Journal of Controlled Release* **2012**, *160*, 117–134.

3. Prabhakar, U.; Maeda, H.; Jain, R. K.; Sevick-Muraca, E. M.; Zamboni, W.; Farokhzad, O. C.; Barry, S. T.; Gabizon, A.; Grodzinski, P.; Blakey, D. C. Challenges and Key Considerations of the Enhanced Permeability and Retention Effect for Nanomedicine Drug Delivery in Oncology. *Cancer Research* **2013**, *73*, 2412–2417.

4. Brown, P. D.; Patel, P. R. Nanomedicine: A Pharma Perspective. *Wiley Interdisciplinary Reviews: Nanomedicine and Nanobiotechnology* **2015**, *7*, 125–130.

5. Cheng, C. J.; Tietjen, G. T.; Saucier-Sawyer, J. K.; Saltzman, W. M. A Holistic Approach to Targeting Disease with Polymeric Nanoparticles. *Nature reviews. Drug discovery* **2015**, *14*, 239–47.

6. Albanese, A.; Tang, P. S.; Chan, W. C. W. The Effect of Nanoparticle Size, Shape, and Surface Chemistry on Biological Systems. *Annual review of biomedical engineering* **2012**, *14*, 1–16.

7. Schmid-Schönbein, G. W.; Usami, S.; Skalak, R.; Chien, S. The Interaction of Leukocytes and Erythrocytes in Capillary and Postcapillary Vessels. *Microvascular research* **1980**, *19*, 45–70.

8. Noguchi, H.; Gompper, G. Shape Transitions of Fluid Vesicles and Red Blood Cells in Capillary Flows. *Proceedings of the National Academy of Sciences of the United States of America* **2005**, *102*, 14159–64.

9. Jiang, X.; Qu, W.; Pan, D.; Ren, Y.; Williford, J.-M.; Cui, H.; Luijten, E.; Mao, H.-Q. Plasmid-Templated Shape Control of Condensed DNA-Block Copolymer Nanoparticles. *Advanced Materials* **2013**, *25*, 227–232.

10. Mao, H. Q.; Roy, K.; Troung-Le, V. L.; Janes, K. a.; Lin, K. Y.; Wang, Y.; August, J. T.; Leong, K. W. Chitosan-DNA Nanoparticles as Gene Carriers: Synthesis, Characterization and Transfection Efficiency. *Journal of Controlled Release* **2001**, *70*, 399–421.

11. Fang, J.; Nakamura, H.; Maeda, H. The EPR Effect: Unique Features of Tumor Blood Vessels for Drug Delivery, Factors Involved, and Limitations and Augmentation of the Effect. *Advanced Drug Delivery Reviews* **2011**, *63*, 136–151.

12. Agarwal, R.; Roy, K. Intracellular Delivery of Polymeric Nanocarriers: A Matter of Size, Shape, Charge, Elasticity and Surface Composition. *Therapeutic delivery* **2013**, *4*, 705–23.

13. Iyer, A. K.; Khaled, G.; Fang, J.; Maeda, H. Exploiting the Enhanced Permeability and Retention Effect for Tumor Targeting. *Drug discovery today* **2006**, *11*, 812–8.

14. Tenzer, S.; Docter, D.; Kuharev, J.; Musyanovych, A.; Fetz, V.; Hecht, R.; Schlenk, F.; Fischer, D.; Kiouptsi, K.; Reinhardt, C.; Landfester, K.; Schild, H.; Maskos, M.; Knauer, S. K.; Stauber, R. H. Rapid Formation of Plasma Protein Corona Critically Affects Nanoparticle Pathophysiology. *Nature nanotechnology* **2013**, *8*, 772–81.

15. Monopoli, M. P.; Åberg, C.; Salvati, A.; Dawson, K. A. Biomolecular Coronas Provide the Biological Identity of Nanosized Materials. *Nature Nanotechnology* **2012**, *7*, 779–786.

16. Hühn, D.; Kantner, K.; Geidel, C.; Brandholt, S.; Cock, I. De; Soenen, S. J. H.; Riveragil, P.; Montenegro, J. M.; Braeckmans, K.; Müllen, K.; Nienhaus, G. U.; Klapper, M.; Parak, W. J. Polymer-Coated Nanoparticles Interacting with Proteins and Cells: Focusing on the Sign of the Net Charge. *ACS Nano* **2013**, *7*, 3253–3263.

17. Madhankumar, A. B.; Slagle-Webb, B.; Wang, X.; Yang, Q. X.; Antonetti, D. a; Miller, P. a; Sheehan, J. M.; Connor, J. R. Efficacy of Interleukin-13 Receptor-Targeted Liposomal Doxorubicin in the Intracranial Brain Tumor Model. *Molecular cancer therapeutics* **2009**, *8*, 648–54.

18. Fenart, L.; Casanova, a; Dehouck, B.; Duhem, C.; Slupek, S.; Cecchelli, R.; Betbeder, D. Evaluation of Effect of Charge and Lipid Coating on Ability of 60-Nm Nanoparticles to Cross an in Vitro Model of the Blood-Brain Barrier. *The Journal of pharmacology and experimental therapeutics* **1999**, *291*, 1017–1022.

19. He, C.; Hu, Y.; Yin, L.; Tang, C.; Yin, C. Effects of Particle Size and Surface Charge on Cellular Uptake and Biodistribution of Polymeric Nanoparticles. *Biomaterials* **2010**, *31*, 3657–66.

20. Kolhar, P.; Anselmo, A. C.; Gupta, V.; Pant, K.; Prabhakarpandian, B.; Ruoslahti, E.; Mitragotri, S. Using Shape Effects to Target Antibody-Coated Nanoparticles to Lung and Brain Endothelium. *Proceedings of the National Academy of Sciences* **2013**, *110*, 10753–

10758.

21. Hume, D. a; Ross, I. L.; Himes, S. R.; Sasmono, R. T.; Wells, C. a; Ravasi, T. The Mononuclear Phagocyte System Revisited. *Journal of leukocyte biology* **2002**, *72*, 621–627.

22. Griffith, J. W.; Sokol, C. L.; Luster, A. D. Chemokines and Chemokine Receptors: Positioning Cells for Host Defense and Immunity. *Annual review of immunology* **2014**, *32*, 659–702.

23. Banquy, X.; Suarez, F.; Argaw, A.; Rabanel, J.-M.; Grutter, P.; Bouchard, J.-F.; Hildgen, P.; Giasson, S. Effect of Mechanical Properties of Hydrogel Nanoparticles on Macrophage Cell Uptake. *Soft Matter* **2009**, *5*, 3984.

24. Perumal, O. P.; Inapagolla, R.; Kannan, S.; Kannan, R. M. The Effect of Surface Functionality on Cellular Trafficking of Dendrimers. *Biomaterials* **2008**, *29*, 3469–76.

25. Wang, J.; Li, L. Coupled Elasticity-Diffusion Model for the Effects of Cytoskeleton Deformation on Cellular Uptake of Cylindrical Nanoparticles. *Journal of the Royal Society, Interface / the Royal Society* **2015**, *12*, 20141023.

26. Akinc, A.; Battaglia, G. Exploiting Endocytosis for Nanomedicines. *Cold Spring Harbor perspectives in biology* **2013**, *5*.

27. Gao, X.; Dong, J.; Zhang, X. The Effect of Nanoparticle Size on Endocytosis Dynamics Depends on Membrane–nanoparticle Interaction. *Molecular Simulation* **2015**, *41*, 531–537.

28. Wang, J.; Li, L.; Zhou, Y. Creep Effect on Cellular Uptake of Viral Particles. *Chinese Science Bulletin* **2014**, *59*, 2277–2281.

29. Gao, H.; Shi, W.; Freund, L. B. Mechanics of Receptor-Mediated Endocytosis. *Proceedings of the National Academy of Sciences of the United States of America* **2005**, *102*, 9469–9474.

30. Jin, H.; Heller, D. a; Sharma, R.; Strano, M. S. Size-Dependent Cellular Uptake and Expulsion of Single-Walled Carbon Nanotubes: Single Particle Tracking and a Generic Uptake Model for Nanoparticles. *ACS nano* **2009**, *3*, 149–58.

31. Shi, W.; Wang, J.; Fan, X.; Gao, H. Size and Shape Effects on Diffusion and Absorption of Colloidal Particles near a Partially Absorbing Sphere: Implications for Uptake of

Nanoparticles in Animal Cells. *Physical Review E - Statistical, Nonlinear, and Soft Matter Physics* **2008**, *78*, 1–11.

32. Li, L.; Liu, X.; Zhou, Y.; Wang, J. On Resistance to Virus Entry into Host Cells. *Biophysical journal* **2012**, *102*, 2230–3.

33. Mosesson, Y.; Mills, G. B.; Yarden, Y. Derailed Endocytosis: An Emerging Feature of Cancer. *Nature reviews. Cancer* **2008**, *8*, 835–850.

34. Harush-Frenkel, O.; Rozentur, E.; Benita, S.; Altschuler, Y. Surface Charge of Nanoparticles Determines Their Endocytic and Transcytotic Pathway in Polarized MDCK Cells. *Biomacromolecules* **2008**, *9*, 435–43.

35. Billiet, L.; Gomez, J.-P.; Berchel, M.; Jaffrès, P.-A.; Gall, T. Le; Montier, T.; Bertrand, E.; Cheradame, H.; Guégan, P.; Mével, M.; Pitard, B.; Benvegnu, T.; Lehn, P.; Pichon, C.; Midoux, P. Gene Transfer by Chemical Vectors, and Endocytosis Routes of Polyplexes, Lipoplexes and Lipopolyplexes in a Myoblast Cell Line. *Biomaterials* **2012**, *33*, 2980–90.

36. Harush-Frenkel, O.; Debotton, N.; Benita, S.; Altschuler, Y. Targeting of Nanoparticles to the Clathrin-Mediated Endocytic Pathway. *Biochemical and biophysical research communications* **2007**, *353*, 26–32.

37. Kirkham, M.; Parton, R. G. Clathrin-Independent Endocytosis: New Insights into Caveolae and Non-Caveolar Lipid Raft Carriers. *Biochimica et biophysica acta* **2005**, *1745*, 273–86.

38. Gonçalves, C.; Mennesson, E.; Fuchs, R.; Gorvel, J.-P.; Midoux, P.; Pichon, C. Macropinocytosis of Polyplexes and Recycling of Plasmid via the Clathrin-Dependent Pathway Impair the Transfection Efficiency of Human Hepatocarcinoma Cells. *Molecular therapy : the journal of the American Society of Gene Therapy* **2004**, *10*, 373–85.

39. Shohdy, K. S.; Alfaar, A. S. Nanoparticles Targeting Mechanisms in Cancer Therapy; Great Efforts, Less Implementations. *Therapeutic Delivery* **2013**, *04*, 1197–1209.

40. Tamura, G.; Shinohara, Y.; Tamura, A.; Sanada, Y.; Oishi, M.; Akiba, I.; Nagasaki, Y.; Sakurai, K.; Amemiya, Y. Dependence of the Swelling Behavior of a pH-Responsive PEG-Modified Nanogel on the Cross-Link Density. *Polymer Journal* **2011**, *44*, 240–244.

41. Gaitzsch, J.; Canton, I.; Appelhans, D.; Battaglia, G.; Voit, B. Cellular Interactions with Photo-Cross-Linked and pH-Sensitive Polymersomes: Biocompatibility and Uptake Studies. *Biomacromolecules* **2012**, *13*, 4188–4195.

42. Raemdonck, K.; Demeester, J.; Smedt, S. De Advanced Nanogel Engineering for Drug Delivery. *Soft Matter* **2009**, *5*, 707.

43. Mercer, J.; Schelhaas, M.; Helenius, A. Virus Entry by Endocytosis. *Annual Review of Biochemistry* **2010**, *79*, 803–833.

44. Perry, J. L.; Reuter, K. G.; Kai, M. P.; Herlihy, K. P.; Jones, S. W.; Luft, J. C.; Napier, M.; Bear, J. E.; Desimone, J. M. PEGylated PRINT Nanoparticles: The Impact of PEG Density on Protein Binding, Macrophage Association, Biodistribution, and Pharmacokinetics. *Nano Letters* **2012**, *12*, 5304–5310.

45. Gref, R.; Lück, M.; Quellec, P.; Marchand, M.; Dellacherie, E.; Harnisch, S.; Blunk, T.; Müller, R. . "Stealth" Corona-Core Nanoparticles Surface Modified by Polyethylene Glycol (PEG): Influences of the Corona (PEG Chain Length and Surface Density) and of the Core Composition on Phagocytic Uptake and Plasma Protein Adsorption. *Colloids and Surfaces B: Biointerfaces* **2000**, *18*, 301–313.

46. Drummond, D. C.; Meyer, O.; Hong, K.; Kirpotin, D. B.; Papahadjopoulos, D. Optimizing Liposomes for Delivery of Chemotherapeutic Agents to Solid Tumors. *Pharmacological reviews* **1999**, *51*, 691–743.

47. Abraham, S. a.; Waterhouse, D. N.; Mayer, L. D.; Cullis, P. R.; Madden, T. D.; Bally, M. B. The Liposomal Formulation of Doxorubicin. *Methods in Enzymology* **2005**, *391*, 71–97.

48. Liu, D.; Poon, C.; Lu, K.; He, C.; Lin, W. Self-Assembled Nanoscale Coordination Polymers with Trigger Release Properties for Effective Anticancer Therapy. *Nature communications* **2014**, *5*, 4182.

49. Wang, H.; Zhao, P.; Su, W.; Wang, S.; Liao, Z.; Niu, R.; Chang, J. PLGA/polymeric Liposome for Targeted Drug and Gene Co-Delivery. *Biomaterials* **2010**, *31*, 8741–8748.

50. Dobay, M. P. D.; Alberola, a. P.; Mendoza, E. R.; Rädler, J. O. Modeling Nanoparticle Uptake and Intracellular Distribution Using Stochastic Process Algebras. *Journal of Nanoparticle Research* **2012**, *14*, 821.

51. Sun, S. X.; Wirtz, D. Mechanics of Enveloped Virus Entry into Host Cells. *Biophysical journal* **2006**, *90*, L10–2.

52. Peetla, C.; Jin, S.; Weimer, J.; Elegbede, A.; Labhasetwar, V. Biomechanics and

Thermodynamics of Nanoparticle Interactions with Plasma and Endosomal Membrane Lipids in Cellular Uptake and Endosomal Escape. **2015**.

53. Anselmo, A. C.; Zhang, M.; Kumar, S.; Vogus, D. R.; Menegatti, S.; Helgeson, M. E.; Mitragotri, S. Elasticity of Nanoparticles Influences Their Blood Circulation, Phagocytosis, Endocytosis and Targeting. *ACS Nano* **2015**, *9*, 3169–3177.

54. Liu, W.; Zhou, X.; Mao, Z.; Yu, D.; Wang, B.; Gao, C. Uptake of Hydrogel Particles with Different Stiffness and Its Influence on HepG2 Cell Functions. *Soft Matter* **2012**, *8*, 9235.

55. Reddy, S. T.; Vlies, A. J. van der; Simeoni, E.; O'Neil, C. P.; Swartz, M. a.; Hubbell, J. a. Exploiting Lymphatic Transport and Complement Activation in Nanoparticle Vaccines. *European Cells and Materials* **2007**, *14*, 103.

56. Abbott, N. J.; Romero, I. a Transporting Therapeutics across the Blood-Brain Barrier. *Molecular medicine today* **1996**, *2*, 106–13.

57. Chan, J. M.; Zhang, L.; Tong, R.; Ghosh, D.; Gao, W.; Liao, G.; Yuet, K. P.; Gray, D.; Rhee, J.-W.; Cheng, J.; Golomb, G.; Libby, P.; Langer, R.; Farokhzad, O. C. Spatiotemporal Controlled Delivery of Nanoparticles to Injured Vasculature. *Proceedings of the National Academy of Sciences of the United States of America* **2010**, *107*, 2213–2218.

58. Peters, D.; Kastantin, M.; Kotamraju, V. R.; Karmali, P. P.; Gujraty, K.; Tirrell, M.; Ruoslahti, E. Targeting Atherosclerosis by Using Modular, Multifunctional Micelles. *Proceedings of the National Academy of Sciences of the United States of America* **2009**, *106*, 9815–9819.

59. Anselmo, A. C.; Modery-pawlowski, C. L.; Menegatti, S.; Kumar, S.; Vogus, D. R.; Tian, L. L.; Chen, M.; Squires, T. M.; Gupta, A. Sen; Mitragotri, S.; Gupta, A. Sen Platelet-like Nanoparticles: Mimicking Shape, Flexibility, and Surface Biology of Platelets To Target Vascular Injuries. *ACS nano* **2014**, *8*, 11243–53.

60. Wang, X.; Li, J.; Wang, Y.; Koenig, L.; Gjyrezi, A.; Giannakakou, P.; Shin, E. H.; Tighiouart, M.; Chen, Z.; Nie, S.; Shin, D. M. A Folate Receptor-Targeting Nanoparticle Minimizes Drug Resistance in a Human Cancer Model. *ACS Nano* **2011**, *5*, 6184–6194.

61. Kim, D.; Lee, E. S.; Oh, K. T.; Gao, Z. G.; Bae, Y. H. Doxorubicin-Loaded Polymeric Micelle Overcomes Multidrug Resistance of Cancer by Double-Targeting Folate Receptor and Early Endosomal pH. *Small (Weinheim an der Bergstrasse, Germany)* **2008**, *4*, 2043–50.

62. Sonvico, F.; Mornet, S.; Vasseur, S.; Dubernet, C.; Jaillard, D.; Degrouard, J.; Hoebeke, J.; Duguet, E.; Colombo, P.; Couvreur, P. Folate-Conjugated Iron Oxide Nanoparticles for Solid Tumor Targeting as Potential Specific Magnetic Hyperthermia Mediators: Synthesis, Physicochemical Characterization, and in Vitro Experiments. *Bioconjugate chemistry* **2005**, *16*, 1181–8.

63. Allen, T. M. Ligand-Targeted Therapeutics in Anticancer Therapy. *Nature Reviews Cancer* **2002**, *2*, 750–763.

64. Elias, D. R.; Poloukhtine, A.; Popik, V.; Tsourkas, A. Effect of Ligand Density, Receptor Density, and Nanoparticle Size on Cell Targeting. *Nanomedicine: Nanotechnology, Biology and Medicine* **2013**, *9*, 194–201.

65. Wardwell, P. R.; Bader, R. a Immunomodulation of Cystic Fibrosis Epithelial Cells via NF-κB Decoy Oligonucleotide-Coated Polysaccharide Nanoparticles. *Journal of biomedical materials research. Part A* **2014**, 1–10.

66. Chakrabarti, A.; Talukdar, D.; Pal, A.; Ray, M. Immunomodulation of Macrophages by Methylglyoxal Conjugated with Chitosan Nanoparticles against Sarcoma-180 Tumor in Mice. *Cellular immunology* **2014**, *287*, 27–35.

67. Dube, A.; Reynolds, J. L.; Law, W.-C.; Maponga, C. C.; Prasad, P. N.; Morse, G. D. Multimodal Nanoparticles That Provide Immunomodulation and Intracellular Drug Delivery for Infectious Diseases. *Nanomedicine : nanotechnology, biology, and medicine* **2014**, *10*, 831–8.

68. Heo, M. B.; Lim, Y. T. Programmed Nanoparticles for Combined Immunomodulation, Antigen Presentation and Tracking of Immunotherapeutic Cells. *Biomaterials* **2014**, *35*, 590–600.

69. Pirollo, K. F.; Chang, E. H. Does a Targeting Ligand Influence Nanoparticle Tumor Localization or Uptake? *Trends Biotechnol.* **2008**, *26*, 552–8.

70. Dai, Q.; Walkey, C.; Chan, W. C. Polyethylene Glycol Backfilling Mitigates the Negative Impact of the Protein Corona on Nanoparticle Cell Targeting. *Angew Chem Int Ed Engl* **2014**, *53*, 5093–5096.

71. Hak, S.; Helgesen, E.; Hektoen, H. H.; Huuse, E. M.; Jarzyna, P. a.; Mulder, W. J. M.; Haraldseth, O.; Davies, C. D. L. The Effect of Nanoparticle Polyethylene Glycol Surface Density on Ligand-Directed Tumor Targeting Studied in Vivo by Dual Modality Imaging. *ACS Nano* **2012**, *6*, 5648–5658.

72. Behr, J. The Proton Sponge: A Trick to Enter Cells the Viruses Did Not Exploit. *CHIMIA International Journal for Chemistry* **1997**, *2*, 34–36.

73. Richter, M.; Steinhilber, D.; Haag, R.; Klitzing, R. Von Visualization of Real-Time Degradation of pH-Responsive Polyglycerol Nanogels via Atomic Force Microscopy. 2018–2022.

74. Zhang, R.; Tang, M.; Bowyer, A.; Eisenthal, R.; Hubble, J. A Novel pH- and Ionic-Strength-Sensitive Carboxy Methyl Dextran Hydrogel. *Biomaterials* **2005**, *26*, 4677–4683.

75. Patton, J. N.; Palmer, A. F. Engineering Temperature-Sensitive Hydrogel Nanoparticles Entrapping Hemoglobin as a Novel Type of Oxygen Carrier. *Biomacromolecules* **2005**, *6*, 2204–2212.

76. Hong, J. S.; Stavis, S. M.; Depaoli Lacerda, S. H.; Locascio, L. E.; Raghavan, S. R.; Gaitan, M. Microfluidic Directed Self-Assembly of Liposome-Hydrogel Hybrid Nanoparticles. *Langmuir* **2010**, *26*, 11581–11588.

77. He, C.; Zhuang, X.; Tang, Z.; Tian, H.; Chen, X. Stimuli-Sensitive Synthetic Polypeptide-Based Materials for Drug and Gene Delivery. *Advanced Healthcare Materials* **2012**, *1*, 48–78.

78. Chen, W.; Zheng, M.; Meng, F.; Cheng, R.; Deng, C.; Feijen, J.; Zhong, Z. In Situ Forming Reduction-Sensitive Degradable Nanogels for Facile Loading and Triggered Intracellular Release of Proteins. *Biomacromolecules* **2013**, *14*, 1214–1222.

79. Hoare, T.; Santamaria, J.; Goya, G. F.; Irusta, S.; Lin, D.; Lau, S.; Padera, R.; Langer, R.; Kohane, D. S. A Magnetically Triggered Composite Membrane for on-Demand Drug Delivery. *Nano Letters* **2009**, *9*, 3651–3657.

80. Lewin, M.; Carlesso, N.; Tung, C. H.; Tang, X. W.; Cory, D.; Scadden, D. T.; Weissleder, R. Tat Peptide-Derivatized Magnetic Nanoparticles Allow in Vivo Tracking and Recovery of Progenitor Cells. *Nature biotechnology* **2000**, *18*, 410–414.

81. Kazakov, S.; Kaholek, M.; Kudasheva, D.; Teraoka, I.; Cowman, M. K.; Levon, K. Poly(N -Isopropylacrylamide- c O -1-Vinylimidazole) Hydrogel Nanoparticles Prepared and Hydrophobically Modified in Liposome Reactors: Atomic Force Microscopy and Dynamic Light Scattering Study. *Langmuir* **2003**, *19*, 8086–8093.

82. Reese, C.; Mikhonin, A.; Kamenjicki, M.; Tikhonov, A.; Asher, S. Nanogel Nanosecond

Photonic Crystal Optical Switching. *Journal of the American Chemical Society* **2004**, *126*, 1493–1496.

83. Schroeder, A.; Kost, J.; Barenholz, Y. Ultrasound, Liposomes, and Drug Delivery: Principles for Using Ultrasound to Control the Release of Drugs from Liposomes. *Chemistry and Physics of Lipids* **2009**, *162*, 1–16.

84. Hoffman, A. S. Hydrogels for Biomedical Applications. *Annals of the New York Academy of Sciences* **2001**, *944*, 62–73.

85. Zha, L.; Banik, B.; Alexis, F. Stimulus Responsive Nanogels for Drug Delivery. *Soft Matter* **2011**, *7*, 5908.

86. Zhang, Z.-M.; Gao, P.-C.; Wang, Z.-F.; Sun, B.-W.; Jiang, Y. DNA Caged Gold Nanoparticle for Controlled Release of Doxorubicin Triggered by DNA Enzyme and pH. *Chemical Communications* **2012**, *00*, 1–3.

87. Hong, J. S.; Vreeland, W. N.; Lacerda, S. H. D.; Locascio, L. E.; Gaitan, M.; Raghavan, S. R. Liposome-Templated Supramolecular Assembly of Responsive Alginate Nanogels. *Langmuir : the ACS journal of surfaces and colloids* **2008**, *24*, 4092–6.

88. An, S. Y.; Bui, M.-P. N.; Nam, Y. J.; Han, K. N.; Li, C. A.; Choo, J.; Lee, E. K.; Katoh, S.; Kumada, Y.; Seong, G. H. Preparation of Monodisperse and Size-Controlled Poly(ethylene Glycol) Hydrogel Nanoparticles Using Liposome Templates. *Journal of colloid and interface science* **2009**, *331*, 98–103.

89. Kazakov, S.; Kaholek, M.; Teraoka, I.; Levon, K. UV-Induced Gelation on Nanometer Scale Using Liposome Reactor. *Macromolecules* **2002**, *35*, 1911–1920.

90. Lin, S.; Sangaj, N.; Razafiarison, T.; Zhang, C.; Varghese, S. Influence of Physical Properties of Biomaterials on Cellular Behavior. *Pharmaceutical research* **2011**, *28*, 1422–30.

91. Bryant, S. J.; Bender, R. J.; Durand, K. L.; Anseth, K. S. Encapsulating Chondrocytes in Degrading PEG Hydrogels with High Modulus: Engineering Gel Structural Changes to Facilitate Cartilaginous Tissue Production. *Biotechnology and Bioengineering* **2004**, *86*, 747–755.

92. Fritze, A.; Hens, F.; Kimpfler, A.; Schubert, R.; Peschka-Süss, R. Remote Loading of Doxorubicin into Liposomes Driven by a Transmembrane Phosphate Gradient. *Biochimica et Biophysica Acta - Biomembranes* **2006**, *1758*, 1633–1640.

93. Zucker, D.; Marcus, D.; Barenholz, Y.; Goldblum, A. Liposome Drugs' Loading Efficiency: A Working Model Based on Loading Conditions and Drug's Physicochemical Properties. *Journal of Controlled Release* **2009**, *139*, 73–80.

94. Haran, G.; Cohen, R.; Bar, L. K.; Barenholz, Y. Erratum: Transmembrane Ammonium Sulfate Gradients in Liposomes Produce Efficient and Stable Entrapment of Amphipathic Weak Bases (Biochim. Biophys. Acta 1151 (1993) 201-215 (BBAMEM 76069)). *Biochimica et Biophysica Acta - Biomembranes* **1994**, *1190*, 197.

95. Murphy, E. a; Majeti, B. K.; Mukthavaram, R.; Acevedo, L. M.; Barnes, L. a; Cheresh, D. a Targeted Nanogels: A Versatile Platform for Drug Delivery to Tumors. *Molecular cancer therapeutics* **2011**, *10*, 972–82.

96. Madhankumar, a B.; Slagle-Webb, B.; Mintz, A.; Sheehan, J. M.; Connor, J. R. Interleukin-13 Receptor-Targeted Nanovesicles Are a Potential Therapy for Glioblastoma Multiforme. *Molecular cancer therapeutics* **2006**, *5*, 3162–3169.

97. Liang, Y.; Kiick, K. L. Multifunctional Lipid-Coated Polymer Nanogels Crosslinked by Photo-Triggered Michael-Type Addition. *Polymer Chemistry* **2014**, *5*, 1728.

98. Csuhai, E.; Kangarlou, S.; Xiang, T.-X.; Ponta, A.; Bummer, P.; Choi, D.; Anderson, B. D. Determination of Key Parameters for a Mechanism-Based Model to Predict Doxorubicin Release from Actively Loaded Liposomes. *Journal of Pharmaceutical Sciences* **2015**, *104*, 1087–1098.

99. Polyansky, A. a; Volynsky, P. E.; Nolde, D. E.; Arseniev, A. S.; Efremov, R. G. Role of Lipid Charge in Organization of Water/Lipid Bilayer Interface: Insights via Computer Simulations. *The Journal of Physical Chemistry B* **2005**, *109*, 15052–15059.

100. Allen, C.; Santos, N. Dos; Gallagher, R.; Chiu, G. N. C.; Shu, Y.; Li, W. M.; Johnstone, S. A.; Janoff, A. S.; Mayer, L. D.; Webb, M. S.; Bally, M. B. Controlling the Physical Behavior and Biological Performance of Liposome Formulations through Use of Surface Grafted Poly (Ethylene Glycol). **2002**, *22*, 225–250.

101. Schillemans, J. P.; Flesch, F. M.; Hennink, W. E.; Nostrum, C. F. Van Synthesis of Bilayer-Coated Nanogels by Selective Cross-Linking of Monomers inside Liposomes. *Macromolecules* **2006**, *39*, 5885–5890.

102. Park, J.; Wrzesinski, S. H.; Stern, E.; Look, M.; Criscione, J.; Ragheb, R.; Jay, S. M.; Demento, S. L.; Agawu, A.; Licona Limon, P.; Ferrandino, A. F.; Gonzalez, D.;

Habermann, A.; Flavell, R. a.; Fahmy, T. M. Combination Delivery of TGF-β Inhibitor and IL-2 by Nanoscale Liposomal Polymeric Gels Enhances Tumour Immunotherapy. *Nature Materials* **2012**, *11*, 895–905.